NUMERICAL INVESTIGATION OF CONCRETE BREAKOUT STRENGTH OF ANCHORS IN SHEAR WITHIN FIBER REINFORCED CONCRETE

By

Yash Hitendrakumar Patel

Supervised by

Dr. Raad Azzawi

Presented to the Faculty of the Graduate School of

The University of Texas at Arlington in Fulfillment

of the Requirements for the Degree of

Master of Science in Civil Engineering

THE UNIVERSITY OF TEXAS AT ARLINGTON

MAY 2020

Arlington, Texas

TABLE OF CONTENTS

LIST OF ILLUSTRATIONS

LIST OF TABLES

Acknowledgments

I would like to offer my sincere appreciation to Dr. Raad Azzawi for his guidance and counsel throughout this research. He has been an incredible mentor to me, providing invaluable professional and academic guidance throughout this research. His knowledge and advice have always provided me with great inspiration and motivation in dealing with technical and academic challenges. I appreciate the time and effort he instilled in my progression through the program and the completion of my thesis. I would also like to thank Nikhil Vasant Moon, Niraj Bora, Harshwardhan Sawaitul, Atheer Al Khafaji, and Mohammed Khanfar, who provided me with invaluable support and assistance throughout this project. Appreciations are also extended to Dr. Warda Ashraf and Dr. Recep Birgul for their valuable advice and guidance. I would like to thank my parents and my sister, who have always provided great encouragement and support, helping me overcome some of the most significant challenges.

May 20, 2020

ABSTRACT

The University of Texas at Arlington, 2020

Supervising Professor: Dr. Raad Azzawi

This study investigates the numerical analysis of concrete breakout strength of cast in place anchors in shear within synthetic fiber reinforced concrete (SYN-FRC). A three dimensional, full-scale model was developed using the ABAQUS 6.14 software. The 3D solid elements with consideration of material nonlinearities were chosen to stimulate the SYN-FRC beam anchorage. The numerical analysis was conducted with a fixed loading rate of 300lb per step to obtain the behavior of fiber-reinforced concrete breakout with design-mix compressive strength of 4,000 psi and fiber volume fraction of 0%, 0.5%, 1.0%, and 1.5%. An inverse analysis was used to calibrate the material model defined in the ABAQUS software with experimental data from previous research since fiber reinforced concrete cannot be modeled precisely with the random distribution of fibers in the concrete matrix. Only compression tests and slump tests were performed to testify the results of the tests with the previous experimental data. Since a good agreement between results was observed, the tensile strength, flexure strength, and anchor shear test results for SYN-FRC were directly used to model in ABAQUS. It was discovered that the compressive strength of the concrete decreased as the fiber reinforcement increased, which can contribute to reducing workability and increased air voids from poor consolidation. In contrast, using synthetic fibers leads to an increase in tensile, flexure, and the anchorage capacity of concrete for the cast-in-place anchor loaded in shear. From the numerical analysis, the Modulus of elasticity increased by 2.8%, 5.0%, and 5.1% for the fiber volume fraction of 0.5%, 1.0%, and 1.5%, respectively, in comparison to the empirical computation of Elastic Modulus. Therefore, from numerical analysis, a parametric study was conducted to evaluate the Elastic Modulus for synthetic fiber reinforced concrete by calibrating load-deflection behavior from physical tests.

Chapter 1

INTRODUCTION

Whether a steel column or a traffic barrier, attaching different elements to concrete through anchorage is classical in the design of different concrete systems. Therefore, it is crucial to understand how the anchors function, and in what manner these anchors can be made more efficient once they are attached to the structural members. When the anchorage equipment was first designed, the beneficial effect of fiber reinforcement, in most cases, was not considered. Taking fiber reinforcement into account might thus give the extra capacity needed to fulfill the requirements of today. In this numerical simulations investigation, the effect of fiber reinforcement on the concrete breakout capacity of cast-in-place headed anchor bolts in concrete structures is studied for single anchors subjected to shear loads. The numerical analyses are performed with the finite element program solver Abaqus/Explicit version 6.10, which is a well-known and thoroughly tested general-purpose finite element modeling program (Dassault Systémes 2010). Experimental results from mechanical testing of headed anchor bolts are the first few in the open literature. Available results from testing of single cast-in headed anchor bolts in the SYN-FRC beam are utilized for validation of used numerical approach and modeling of the concrete material.

There are different kinds of anchors used in the civil industry. The main distinction includes cast-in-place and post-installed anchors. The cast-in-place anchor is placed within the concrete pour, locking it in place as the concrete cures while the post-installed anchor is installed into concrete that has already cured. Some anchors are also designed using adhesives to create a bond between steel and concrete, which holds the anchor in place. The principle of concrete anchorage is essentially the same irrespective of the type of anchors. The anchor has a volume of concrete, otherwise known as a "cone of influence" that holds the anchor in place. This influenced concrete resists forces, such as tension and shear that threaten to tear the anchor away from the concrete. A concrete breakout occurs when the force resisted by the cone of influence is too high and exceeds the strength limits

of concrete. Often the anchor itself, or even the adhesive bond, can fail before a concrete breakout occurs. Concrete anchorage breakout is controlled by many different aspects, such as the method of installation, the spacing, the embedment, the edge distance, or even the type of anchors. As the confinement of fibers increases in concrete around the anchors, the cone of influence increases.

A sizable amount of past research has been dedicated to synthetic fiber-reinforced concrete (SYN-FRC) due to its capability to enhance the existing concrete design methods and practices. In particular, propylene fibers are non-corrosion, making them more beneficial than other steel fiber products. Additionally, SYN-FRC is known to provide ease in construction, which allows a reduction of cracks developed throughout the design life of a concrete member. If SYN-FRC can stay uncracked throughout its design life and increases the concrete tensile and flexure strength, then using fibrous concrete for anchorage could be advantageous.

1.1 Objectives

The main objective of this study is to numerically investigate the concrete breakout strength for steel headed anchors in shear within synthetic fiber reinforced concrete of varying dosages using finite element software, ABAQUS. Parameters of interest for this study are the effects on breakout strength, compressive strength, Modulus of elasticity, and concrete constitutive model of fiber reinforced concrete with the different volume fraction of polypropylene fibers as well as mesh size and type of boundary conditions in finite element models. Other issues of interest are the interaction of local stress field in the vicinity of the anchor and global stress field in the concrete structure, the possibility to transmit mechanical loads from the embedded anchors to the concrete and how to perform analytical modeling and analysis of mechanically loaded anchors in shear within fiber reinforced concrete structures. Four SYN-FRC concrete models were designed and analyzed to meet these objectives. A study on the effect of Modulus of Elasticity was also performed to compare with strength properties of concrete and increasing fiber dosage. An approach to computing Elastic Modulus for SYN-FRC was developed by calibrating the load-deflection behavior of numerical results with experimental outcomes.

1.2 Research Contribution

The benefits of this research study include the possible reduced design cost and increased concrete breakout strength of anchor in shear by the simple addition of fibers. For applications such as anchorage to the fiber-reinforced pavement for guardrails, steel column anchorage to the concrete foundation, and various other, this research allows the engineers to design and analyze the additional strength provided by the fiber reinforcement. The additional strength provided by the fibers to concrete allows a better performance of concrete while still maintaining the necessary strength requirements. Moreover, research on the computation of Elastic Modulus of SYN-FRC can improve on the results found through numerical analysis, as discussed in this study.

1.3 Outline for Dissertation

This thesis is organized into the six following chapters, respectively:

Chapter 1 – Introduction: This chapter explains the nature of concrete in shear and why fibers have been introduced to the concrete mixture. It also explains the parameters of interest for the numerical analysis of SYN-FRC Beam Anchorage.

Chapter 2 – Literature Review: This chapter presents the background of anchorage to concrete, fiber reinforced concrete and previous studies on finite element analysis of fiber reinforced concrete.

Chapter 3 – Experimental Program: This chapter presents material and properties, the concrete mixture design, the slump and compressive tests, and the adoption of the experimental set-up and results from previous research to model in ABAQUS.

Chapter 4 – Finite Element Modeling: Describes the modern development of FEM and the steps to model an SYN-FRC Beam Anchorage in ABAQUS.

Chapter 5 – Numerical Analysis: Analyze the resistance force and provides a load-displacement curve comparison of experimental and numerical results. It also suggests an equation to compute Elastic Modulus for SYN-FRC compared to plain concrete for numerical analysis.

Chapter 6 – Summary and Conclusion: Concludes how the objectives of this research are satisfied. It also provides further recommendations for this research and the overall benefits of SYN-FRC Beams Anchorage.

Chapter 2

LITERATURE REVIEW

2.1 Previous Research and Accepted Design Practices

2.1.1 Concrete Anchors

Concrete anchors are widely used in the construction of bridges, buildings, and power transmission towers. Various types of anchors have been developed over the past 40 years. The behavior of anchors has been extensively studied (CEB, 1997; Cannon, 1995a and b; Cook et al., 1989; Klingner et al., 1982; and Eligehausen et al., 2006), and the results have been implemented in design codes (ACI 318-08; FIB, 2008).

There are only two main divisions of concrete anchors: cast-in-place and post-installed. Like the name suggests, cast-in-place anchors, such as hex head bolts or J bolts, are set in place as the concrete is molded. Once the concrete cures, the anchors are set in place and can be used. Cast-in-place anchors are standard in applications such as pre-cast design and can be used in groups of anchors connected via a steel base plate. Post-installed anchors are installed after the concrete has cured. These anchors are installed via drilling into the concrete and then applying adhesive to the anchor bolt, torqued into place, etc.as shown in Figure1, depending on the type of post-installed anchor bolt used. Post-installed anchors are much more versatile than cast-in-place bolts since they can be installed after the concrete has cured.

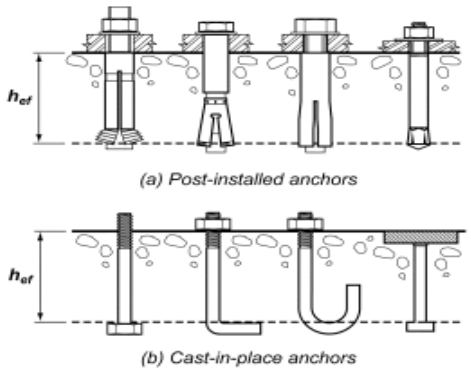

Figure 1. Types of anchors

Before the further investigation, it is essential to understand the different possible modes of failure if the member is subjected to shear force. Figure 2 from ACI 318M-14 shows the possible failure modes of an anchor in shear loadings.

The ACI-318-14 Appendix-D allows the designs of anchors and guides in calculating the three different types of anchorage failures under shear loading: steel failure (D.6.1), pryout failure (D.6.3), and concrete breakout (D.6.2).

The exposed portion of an anchor (also called a lever arm as in Eligehausen et al., 2006) causes a moment and sometimes tension in the anchor shaft when subjected to shear. The shear capacity of exposed anchor bolts in concrete is thus affected by the exposed length, anchor bolt diameter, and other factors such as restraints of anchor end rotations. The exposed portion of an anchor, as reported by Petersen (2011), also changes the fracture process of the anchor. For our analysis, long embedment and edge distance of the anchors is considered, so there is steel shear failure, but still, we have a definite effect of concrete strength on the failure, based on ACI-318-14.

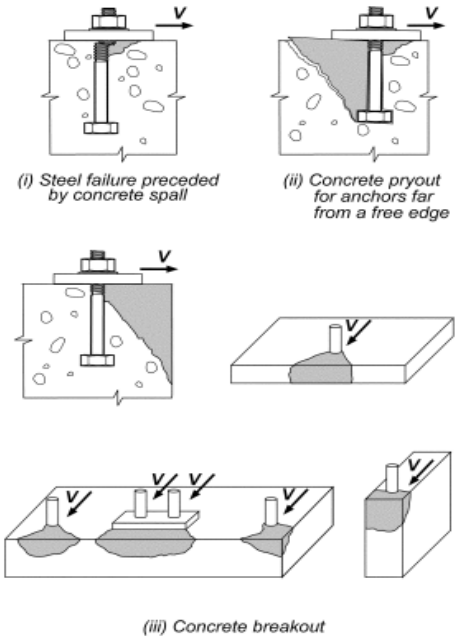

Figure 2. Types of failure under shear loading

To prevent such anchors failures, it should be designed accordingly. In this article, the code requirements are outlined in Chapter 27 of ACI 318M-14 or Appendix D of ACI 318M-08: Anchoring to Concrete. It is a two-part article for the design considerations under shear loading on anchoring to concrete. To sum it up, the following are the general requirements for the strength of anchors.

Anchors failure under shear load as per ACI 318M-14-Appendix-D,

1- Steel failure,

Steel failure is the rupture of the shank of the anchor. As the shear load increases on the anchor and anchor may begin to yield, and the cross-sectional area starts to pinch together and decrease. If the shear load continues to grow and surpass the ultimate shear strength of the anchor, the anchor gets fractured. The ACI code currently prescribes equation utilizing the maximum strength of the steel, as opposed to the yielding strength. Equation 1 is the accepted equation for a nominal strength of an anchor bolt for shear Vsa shall not exceed (a) through (c):

(a) For cast-in headed stud anchor,

$$Vsa = n*Ase,v * futa \quad \text{……..……...(1)}$$

Steel strength in anchor design equation (ACI 17.5.1.2a)

(b) For cast-in headed bolt and hooked bolt anchors and for post-installed anchors where sleeves do not extend through the shear plane,

$$Vsa = n*0.6 * Ase,v * futa \quad \text{…..……..……(2)}$$

Steel strength in anchor design equation (ACI 17.5.1.2b)

Where ***Ase,V*** is the effective cross-sectional area of an anchor in shear, $in.^2$, and ***futa*** shall not be taken greater than the smaller of **1.9*fya*** and 125,000 psi.

(c) For post-installed anchors where sleeves extend through the shear plane, ***Vsa*** shall be based on the results of tests performed and evaluated according to ACI 355.2. Alternatively, Eq. (17.5.1.2b) shall be permitted to be used.

2- Pryout failure,

(Fuchs, W.; Eligehausen, R.; and Breen, J. 1995) A pryout failure may theoretically only occur if the ratio of anchorage depth to anchor diameter is minimal, and the tensile capacity is deficient. In contrast, in shear, a brittle concrete failure occurs for fastenings located close to the edge and cannot be avoided by increasing anchorage depth. Steel failure, often proceeded by a local concrete spall in front of the anchor, is observed for fasteners sufficiently far away from the edge. For that case, the load-displacement behavior depends on the ductility of the anchor steel. A concrete pryout-type failure of fastening located quite far away from the edge may occur for single anchors and especially for groups of anchors with a small ratio of embedment depth to anchor diameter and high tensile capacity.

The pryout mechanism for cast-in anchors usually occurs with very short, and stocky studs welded to a steel plate or beam flange. The studs are typically so short and stiff that under a direct shear load, they bend primarily in single curvature. The ensuing deformation results in the “heel” of the stud head “kicking back,” which breaks out a crater of concrete behind the stud. Internal bearing pressures develop in the concrete near the concrete surface at the stud weld and the stud head due to rotational restraint. This failure mechanism occurs away from all edge effects when the anchorage is located “in-the-field” of the member.

The behavior is somewhat analogous to a laterally loaded pile on earth. A longer and less stiff stud behaves differently. The longer and deeper embedded stud bend in

double curvature and the deeply embedded head portion of the stud remains nearly stationary or fixed in the concrete. At the junction of the headed stud and plate, the projected stud diameter of the stud bears directly on the concrete near the surface and induces a zone of concrete crushing. If the connection is close to an edge, the concrete anchorage assembly is likely to break out a concrete section due to the edge effects. If the connection is located sufficiently away from the edge to preclude an edge breakout, the stud likely fails in a steel shear failure mode, the shear capacity of the stud group clear of the edge effects can be defined by:

$$Vs = n * As * fut \quad \text{.....(3)}$$

Shear capacity of the stud group clear of the edge equation

Vs = nominal shear strength of a single-headed stud or group of headed studs governed by steel strength (lb), n = number of studs or anchors in a group, As = effective cross-sectional area of a stud anchor (sq in.), and fut = design minimum tensile strength of headed stud steel in tension (psi) Currently, this equation is the same as Eq. D-17 of ACI 318-05 Appendix D,1 without the capacity reduction factor, φ.

3- Concrete breakout strength of anchor in shear

The nominal concrete breakout strength in shear, ***Vcb*** of a single anchor or ***Vcbg*** of a group of anchors, shall not exceed:

(a) For shear force perpendicular to the edge on a single Anchor

$$Vcb = Avc/Avco * \psi ed,v * \psi c,v * \psi h,v * Vb \quad \text{.....(4)}$$

Nominal concrete breakout strength in shear equation (ACI 17.5.2.1a)

(b) For shear force perpendicular to the edge on a group of anchors

$$Vcbg = Avc/Avco * \psi ec,v * \psi ed,v * \psi c,v * \psi h,v * Vb \quad \text{.....(5)}$$

Nominal concrete breakout strength in shear equation (ACI 17.5.2.1b)

(c) For shear force parallel to an edge, ***Vcb*** or ***Vcbg*** shall be permitted to be twice the value of the shear force determined from Eq. (17.5.2.1a) or (17.5.2.1b), respectively, with the shear force assumed to act perpendicular to the edge and with $\psi_{ed,V}$ taken equal to 1.0.

(d) For anchors located at a corner, the limiting nominal concrete breakout strength shall be determined for each edge, and the minimum value shall be used.

Anchor bolts under shear loads, and located without a nearby free edge in the direction of load, can fail by local crushing of the concrete under bearing stresses from the anchor bolt; by pryout of the head of the anchor in a direction opposite to the direction of applied load, or by yield and fracture of the anchor bolt steel.

2.1.2 Polypropylene Fiber Reinforced Concrete

(Dharan D. and Lal A. 2016) Fiber-reinforced concrete (SYN-FRC) is concrete containing fibrous material, which increases its structural integrity. The character of fiber-reinforced concrete changes with varying concretes fiber materials, geometries, distribution, orientation, and densities. Polypropylene fiber is a lightweight synthetic fiber. It prevents crack formation and reinforces the concrete structure. In this project work polypropylene fibers (Blended type) of different percentage (0.5%, 1%, 1.5%, and 2%) added in concrete. Tests on workability, compressive strength, flexural resistance, split tensile strength, and Modulus of Elasticity were conducted on specimens.

The fiber dispersion into concrete is one of the methodologies to improve the strength properties of concrete. Polypropylene fibers are synthetic fibers obtained as a by-product of the textile industry. These are available in different aspect ratios and are economical in cost. Polypropylene fibers are characterized by low specific gravity and low cost. Its use enables reliable and effective utilization of intrinsic tensile and flexural strength of the material along with a significant reduction of plastic shrinkage cracking and minimizing of thermal cracking.

It provides reinforcement and protects the damage of concrete structure and prevents spalling in case of fire. The fibers are manufactured either by the pulling wire procedure with circular cross-section or by extruding the plastic film with a rectangular cross-section. They appear either as fibrillated bundles, monofilament. The fibrillated polypropylene fibers are formed by the expansion of a plastic film, which is separated into strips and then slit. The fiber bundles are cut into specified lengths and fibrillated. In monofilament fibers, the addition of buttons at the ends of the fiber increases the pull-out load.

(Mohod M. et al. 2015) This study presents an experimental approach to the performance of polypropylene fiber reinforced concrete. It deals with the effects of the addition of various proportions of polypropylene fibers on the properties of High strength concrete. An experimental program was carried out to explore its effects on compressive, tensile, flexural strength under different curing conditions. The main aim of the investigation program is to study the effect of Polypropylene fiber mix by varying content such as 0%, 0.5%, 1%, 1.5% & 2%, and finding the optimum Polypropylene fiber content. A notable increase in the compressive, tensile, and flexural strength was observed. However, further investigations were highly recommended and should be carried out to understand the more mechanical properties of fiber-reinforced concrete.

(Aslani F. and Samali B. 2014) Concrete is an inherently brittle material with a relatively low tensile strength compared to compressive strength. Reinforcement with randomly distributed short fibers presents a practical approach to the stabilization of the crack and improving the ductility and tensile strength of concrete. A variety of fiber types, including steel, synthetics, and natural fibers, have been applied to the concrete. Polypropylene (PP) fiber reinforcement is considered to be an effective method for improving the shrinkage cracking characteristics, toughness, and impact resistance of concrete materials.

(Ramujee K. et al. 2013) In this study, the results of the Strength Properties of Polypropylene fiber reinforced concrete have been presented. The compressive strength, splitting tensile strength of concrete samples made with different fibers amounts varies from 0%, 0.5%, 1% 1.5% and 2.0% were studied. The samples with added Polypropylene fibers of 1.5 % showed better results in comparison with the others.

Effect of Polypropylene Fibers in Concrete,

(Dharan D. and Lal A. 2016) Cracks play an essential role as they change concrete structures into permeable elements and, consequently, with a high risk of corrosion. Cracks not only reduce the quality of concrete and make it aesthetically unacceptable but also make structures out of service. If these cracks do not exceed a certain width, they are neither harmful to a structure nor its serviceability. Therefore, it is crucial to reduce the crack width, and this can be achieved by adding polypropylene fibers to concrete. Thus the addition of fibers in cement concrete matrix bridges these cracks and restrains them from further opening. To achieve deflection in the beam, additional forces and energies are required to pull out or fracture the fibers. This process, apart from preserving the integrity of concrete, improves the load-carrying capacity of a structural member beyond cracking.

Fibers are usually used in concrete to control plastic shrinkage cracking and drying shrinkage cracking. They also lower the permeability of concrete and thus reduce the bleeding of water. Some types of fibers produce a more significant impact, abrasion, and shatter resistance in concrete. Generally, fibers do not increase the flexural strength of concrete, so it cannot replace moment resisting or structural steel reinforcement. Some fibers reduce the strength of concrete. The amount of fibers added to a concrete mix is measured as a percentage of the total volume of the composite (concrete and fibers) termed volume fraction (V_f). V_f typically ranges from 0.1 to 3%. Aspect ratio (l/d) is calculated by dividing fiber length (l) by its diameter (d). Fibers with a non-circular cross-section use an equivalent diameter for the calculation of aspect ratio.

If the Modulus of Elasticity of the fiber is higher than the matrix (concrete or mortar binder), they help to carry the load by increasing the tensile strength of the material. An increase in the aspect ratio of the fiber usually segments the flexural strength and toughness of the matrix. However, fibers that are too long tend to “ball” in the mix and create workability problems. Some recent research indicated that using fibers in concrete has a limited effect on the impact resistance of concrete materials. This finding is significant since traditionally, people think the ductility increases when concrete reinforced with fibers. The results also pointed out that the microfibers are better in impact resistance compared with the longer fibers.

Many studies have been conducted on the change in material properties in concrete with the addition of fiber reinforcement. Studies have shown that with the introduction of fiber reinforcement, the tensile and flexural strength subsequently increases (Ramli, 2011). The fibers embedded within the concrete further bind the aggregate together. The tensile strength of typical concrete is rather low. Regular concrete is bound together by chemical bonds created between cement and aggregate through hydration. The chemical bonds binding regular concrete together do not have strong tensile strength, and as regular concrete is pulled apart, the concrete cracks and fails quickly. As fibers are introduced to the concrete mixture, the fibers further confine the concrete and bind it together. As a shear and tensile force act upon fiber reinforced concrete, both the chemical bonds and the fiber bind the concrete together, resulting in a higher tensile strength (ft.). Likewise, as the tensile strength of the concrete increases, so does the flexural strength. Since the fiber reinforced concrete can withstand higher tensile stresses, increasing flexure resulting in higher shear and tensile stresses can also be resisted.

Furthermore, compressive strengths of fiber reinforced concrete have also been documented as slightly increasing, or no effects with the addition of fiber reinforcement

(Ramli, 2011). This is due to the confining effects of the fiber on the concrete's aggregate. However, as the dosage of fiber increases, the workability of the concrete typically decreases. Once enough fiber has been added to a concrete mixture, the workability of the concrete may be too low to place, compact properly, and consolidate. If the workability is too low and the concrete is not consolidated correctly, small air voids may be present within the cured concrete. These air voids can lead to a reduction in the compressive strength of the concrete.

There are several varieties of fiber reinforcement, including steel and polypropylene fibers. Steel fibers are commonly used in the design of fiber-reinforced pavement to reduce the cracking of the concrete due to exposure and service loading. Steel fibers, however, are susceptible to rust. Polypropylene fibers are synthetic fiber with similar effects to the mechanical properties of concrete but cannot rust. Both steel and polypropylene fibers can be used to replace small reinforcing bars such as #3 or #4 rebar (MasterFiber MAC Matrix).

2.1.3 Fiber Reinforced Concrete Anchorage

There have been past studies focusing on the anchorage to fiber reinforced concrete. One study performed in Iraq focuses on the use of cast-in-place anchor bolts embedded within steel fiber reinforced concrete (Al-Taan, 2011). The anchor bolts were embedded at varying depths in concrete with varying amounts of fiber reinforcement.

It was discovered that the failure angle was influenced by the embedment depth, the amount of fiber reinforcement, and the compressive strength of the concrete. As the embedment depth and fiber reinforcement increase, the angle of failure increased. As the concrete compressive strength decrease, the angle of failure decreased. Their results also showed an overall increase in the tensile strength of an anchor with increasing amounts of fiber reinforcement.

2.1.4 Numerical Analysis of Fiber Reinforced Concrete

(Azzawi R. and Varughese N. 2020) This research investigates the behavior of encased steel composite beams within steel fiber reinforced concrete (SFRC) in straight and preflex beams, using nonlinear analysis. ABAQUS FEA software has been adopted. Composite steel beams encased in fiber reinforced concrete are analyzed, and a comparison is made with available experimental results. Good agreement with the experimental results is observed. The upwards camber of the steel section is introduced on the steel joist. It's found that the preflex section can increase the ultimate load capacity by 10% and decrease midspan displacement by 13% of the same beams without the preflex steel section. Steel fiber dosages, compressive strength, Modulus of rupture are examined. The effect of cambering and mesh refinement is also investigated.

(Abolmaali A., Mostafazadeh M. and Ghahremannejad M. 2019) This study presents experimental and numerical investigations of the shear strength of synthetic fiber-reinforced concrete (SYN-FRC) box culverts. Shear and flexure material tests associated with numerical analysis were conducted to obtain the material properties of concrete with compressive strength of 34MPa (5,000 psi) and a synthetic volume fraction of 0.52%. The material tests showed that the shear and flexure strength of SYN-FRC were higher than those of plain concrete (without adding fiber). The flexure material test showed that SYN-FRC could carry load even after concrete cracking, unlike the plain concrete, which collapses immediately after cracking. Besides, four full-scale SYN-FRC box culverts were tested in the laboratory, and numerical models were calibrated using experimental data. All specimens failed in the shear failure mode associated with an inclined shear crack from the tip of the haunch to the middle of the loading plate. The results demonstrated that synthetic fibers could be a viable alternative to shear transverse reinforcements. Additionally, numerical verification of SYN-FRC box culverts validates the use of concrete, brittle, cracking material models for simulating SYN-FRC in the finite element method (FEM).

(Ozbolt J., Gambarelli S. and Hoffman J. 2017) In this research, the results of a 3D finite element parametric study for a single bonded anchor loaded under sustained tensile load are presented and discussed. The numerical model is first calibrated based on the experimental tests, and subsequently, the parametric study is carried out. The influence of geometry, fracture properties, and creep of concrete and chemical adhesive (epoxy) on the behavior of anchors under sustained load is investigated. The study shows that the fracture of concrete and its interaction with the creep of concrete has a dominant influence on the resistance and behavior of anchors under sustained load. Moreover, the behavior of bonded anchors under sustained load is more sensitive if the ratio between the strength of chemical adhesive and concrete increases. It is shown that the most critical situation is the use of high-quality polymer in low-quality concrete.

(Smolcic Z. and Ozbolt J. 2014) This study carries out an experimental and numerical analysis of hook-end steel fiber reinforced concrete. The experimental tests are performed on notched beams loaded in 3-point bending using fiber volume fractions up to 1.5 %. The numerical analysis of fiber-reinforced concrete beams is performed at the mesoscale. The concrete is discretized with 3D solid finite elements, and a Microplane model is used as a constitutive law. The fibers are modeled by randomly generated 1D truss finite elements, and the interface between concrete and fibers is simulated by employing a discrete bond-slip relationship. The analysis realistically replicates experimental results. In all investigated cases, failure is due to the pull-out of fibers. It is shown that with the increase of volume content of fibers, the adequate bond strength and slip capacity of fibers decreases.

Chapter 3

EXPERIMENT PROGRAM

3.1 General

In the year of 2019, a research project at the University of Texas was carried out to obtain information to determine the concrete breakout strength of anchors in shear within fiber reinforced concrete (Khanfar M. et al. 2019). To determine the compression, split, and flexure strength of fiber reinforced concrete, the test was performed under the ASTM C39 compression test, ASTM C496 split tensile test, and ASTM C78 flexure test. The compression tests performed utilized small 4”x8” cylinders. The split tests were also performed using 4”x8” cylinders. The flexure tests required 6”x6”x20” beams (Khanfar M. et al. 2019).

The anchor shear tests required beams that would be large enough to ensure that the anchors would have sufficient spacing because the test was conducted for a single anchor, not in a group, and deep enough to ensure adequate bearing area that resists the shear force. For these reasons, a large 54”x24”x18” beam was chosen as the anchor specimens’ size. The large beam would allow multiple anchors to be sufficiently spaced with minimal possibility of breaking through another nearby anchor’s influence area (Khanfar M. et al. 2019).

3.2 Materials and Properties

BASF Chemical Company’s (BASF Chemical Company 2012) macro synthetic fibers, made from a blend of polypropylene resins, met the requirements of ASTM C1116 and were used for this study. Figure 3 gives the physical properties of the fibers. Typically, synthetic fibers are used for reinforcing concrete to control shrinkage, temperature, and settlement cracking; increase flexural toughness and impact resistance; and improve residual strength, durability, and cohesion (BASF Chemical Company 2012). Figure 4

presents the type of fiber applied in this research. Fibers were added to the mixture following the manufacturer's specifications.

Property	Value
Specific gravity	0.91
Melting point	160°C (320°F)
Ignition point	590°C (1,094°F)
Absorption	Nil
Alkali resistance	Excellent
Tensile strength	585 MPa (85 Ksi)
Length	54 mm (2.1 in.)
Aspect ratio	67
Fiber type	Embossed
Material	100% virgin polypropylene
Chemical resistance	Excellent
Modulus of elasticity	6,900 MPa (1,000 Ksi)
Density	908 kg/m^3 (1,530 lb/yd^3)

Figure 3. Physical properties of polypropylene fiber (synthetic fibers)

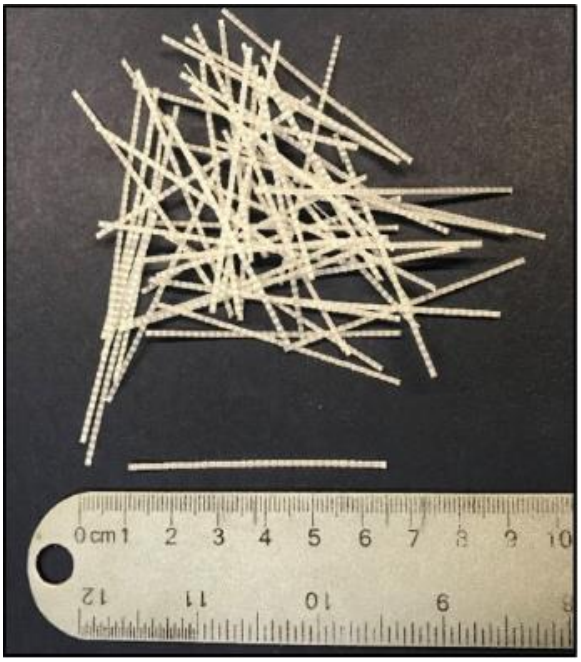

Figure 4. MasterFiber MACMatrix synthetic fibers

To affirm the test results for the fiber-reinforced concrete from previous research to utilize it for ABAQUS modeling, only compression tests and slump tests were performed.

For the split tensile test and flexure test, the results were directly obtained from the previous research (Khanfar M. et al. 2019).

3.2.1 Slump Test

Slump tests were performed per ASTM C143. These tests used an 8” base, 4” top 12” tall slump cone. Concretes from all four mix designs were poured into the cone, filling the cone in three lifts. After each lift, the cone was rodded 25 times. Once the cone was filled to the top, the cone was carefully lifted.

The concrete crumbled downward or “slumped” and the slump was measured from the top of the cone using a tape measure. The slump of 6.5 in., 6.2 in., 5.8 in. and 5.4 in. was found for 0%, 0.5%, 1.0% and 1.5% fiber reinforcement respectively. It was discovered that the slump would decrease as more fibers were added to the mixture. The workability of the mixtures was also seen to decrease as more fibers were introduced to the mixture. The slump test performed can be seen in Figures 5 and 6.

Figure 5. Filled slump cone

Figure 6. Slump test

3.2.2 Compression Test

Table 1-4 presents the mix design for 4,000 psi compressive strength dry-cast concrete, to which synthetic fiber by volume fraction was added. The synthetic fibers were introduced into the mixer after all of the cement, sand, and coarse aggregate had been thoroughly dried mixed. Then the water was gradually added to the mixer. This approach was taken to ensure uniform distribution of the fibers throughout the entirety of the mixture. Fresh concrete was poured into molds and compacted with rammers. For each fiber dosage (0%, 0.5%, 1.0%, and 1.5%), three 4" x 8" long cylinders were made for the compression test in accordance with ASTM C39. Figure 7-9 shows the preparation of the test specimen and set-up for the compression test.

Table 1. 0% Fiber Concrete Design Mixture

0% Fiber Concrete Design Mixture				
Component	ASTM	Density (lbs/cf)	Weight (lbs)	Volume (cf)
Type I/II Cement	C150	196.6	541	2.75
#67 Size Coarse Aggregate	C33	167.3	1885	11.27
Concrete Sand	C33	163.6	1458	8.91
Water		62.4	254	4.06
Polypropylene Fiber		59.06	0	0
Concrete		153.3	4138	27

Table 2. 0.5% Fiber Concrete Design Mixture

0.5% Fiber Concrete Design Mixture				
Component	ASTM	Density (lbs/cf)	Weight (lbs)	Volume (cf)
Type I/II Cement	C150	196.6	534	2.72
#67 Size Coarse Aggregate	C33	167.3	1880	11.24
Concrete Sand	C33	163.6	1452	8.88
Water		62.4	251.2	4.03
Polypropylene Fiber		59.06	7.973	0.14
Concrete		152.8	4125	27

Table 3. 1.0% Fiber Concrete Design Mixture

1.0% Fiber Concrete Design Mixture				
Component	ASTM	Density (lbs/cf)	Weight (lbs)	Volume (cf)
Type I/II Cement	C150	196.6	527.4	2.68
#67 Size Coarse Aggregate	C33	167.3	1874	11.2
Concrete Sand	C33	163.6	1447	8.84
Water		62.4	249.1	3.99
Polypropylene Fiber		59.06	15.95	0.27
Concrete		152.4	4113	27

Table 4. 1.5% Fiber Concrete Design Mixture

1.5% Fiber Concrete Design Mixture				
Component	ASTM	Density (lbs/cf)	Weight (lbs)	Volume (cf)
Type I/II Cement	C150	196.6	520.7	2.65
#67 Size Coarse Aggregate	C33	167.3	1869	11.17
Concrete Sand	C33	163.6	1441	8.81
Water		62.4	247	3.96
Polypropylene Fiber		59.06	23.92	0.41
Concrete		152	4101	27

Figure 7. Specimen cast for Compression test

Figure 8. Capping of Specimens for Compression test

Figure 9. Compression test

3.2.3 Tensile and Flexure Test

The Tensile and Flexure test was not conducted for this study, as this research focuses mainly on numerical simulations. However, the results for the tensile tests and flexure tests were directly obtained from previous research (Khanfar M. et al. 2019).

3.2.4 Physical test of Anchor bolt in shear

The test setup for the physical tests is visually described in Figure 10-12. As seen in Figure 10, the vertical displacement was applied by a hydraulic ram. Centered in the test frame, the hydraulic ram is connected to a steel plate in which the anchor bolt is attached. The magnitude of the corresponding force caused by the applied displacement was measured in the load cell, and the displacement was registered by a linear potentiometer on the Anchor rod, see Figure 11.

For the static tests, the displacement was applied in a monotonically increasing manner so that failure occurred in two to four minutes to avoid dynamic effects. Once the machine starts to apply the load, the vertical displacement of the steel plate creates pure shear in anchor specimen. The anchor bolt was tested individually, single anchor not group (Khanfar M. et al. 2019).

Figure 10. Load cell placement (Khanfar M. et al. 2019)

Linear Variable Differential Transformers (LVDT) was used for measuring the displacement of the anchors, LVDT attached with the 16" steel plate, and adjusted to be vertical. Once the anchor starts to deflect, the LVDT starts measuring displacement where the sensor is touched to the top of the compression machine that supports the specimen's set-up, as seen in Figure 12. The load ratio applied is 300 lb/min.

Figure 11. Linear Variable Differential Transformers (LVDT) placement
(Khanfar M. et al. 2019)

Figure 12. Linear Variable Differential Transformers (LVDT) and Load Cell Setup
(Khanfar M. et al. 2019)

3.3 Tests and Results

Table 5. Load Results for Compression Test

Compression Test Failure load (lbs)				
Fiber Volume Fraction (%)	0%	0.50%	1.00%	1.50%
Specimen #				
1	43005	42069	37650	35187
2	46358	43890	36786	34538
3	47678	41300	36404	33888

Table 6. Results for Compressive Strength

Compressive Strength (psi)				
Fiber Volume Fraction (%)	0%	0.50%	1.00%	1.50%
Specimen #				
1	3830	3349	2998	2802
2	3582	3494	2929	2750
3	3797	3288	2898	2698
Average	3736	3377	2942	2750

Table 7. Results Comparison for compression test and adoption of Tensile and Flexure test results

Experimental Results				
Fiber Volume Fraction (%)	0%	0.50%	1.00%	1.50%
Compressive strength (psi)	3736	3377	2942	2750
Compressive strength (psi) (Khanfar M. et al. 2019)	3649	3245	2707	2658
Tensile Strength (psi) (Khanfar M. et al. 2019)	135.3	163.8	195.1	214
Modulus Rupture (psi) (Khanfar M. et al. 2019)	412.4	477.7	536.6	653.2

Chapter 4

FINITE ELEMENT MODELLING

4.1 General

Finite Element Analysis (FEA) is the numerical approach to divide a single body into finite elements to investigate the behavior of the entire body at the same time interaction between these small elements. The finite element model comprises a SYN-FRC beam, an anchor attached to a steel plate, as seen in Figure 30.

The objective has been to achieve numerical simulation results in compliance with the mentioned physical test results by using the constitutive material model described in chapter 3. The methodology has thenceforth been to use the established model for further numerical simulations of other similar problems. Single anchor bolts in fiber reinforced concrete have been investigated using finite element analyses. Within the scope of this project regarding anchors loaded in shear, numerical simulations have been performed based on the above mentioned physical tests. The finite element model, the constitutive material model, and results from the numerical simulations are presented in this chapter.

As the simulation results show good agreement with physical test results, the constitutive material model utilized in the simulations is considered appropriate for the task at hand. Nevertheless, different parameters defining the constitutive model have been examined in a parametric study to see what impact on analysis results different parameters may have.

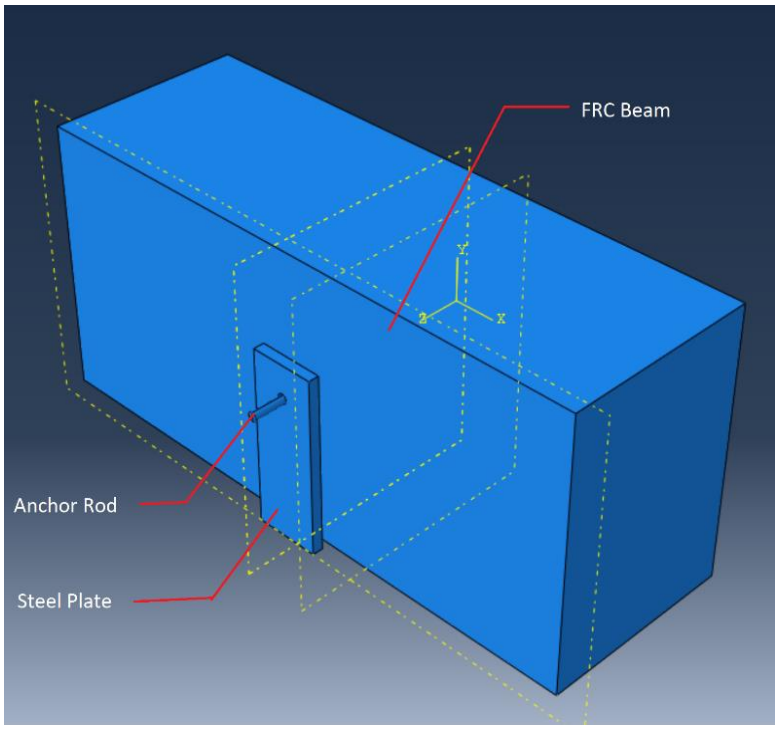

Figure 13. ABAQUS- Perspective view of the different parts constituting the model

The SYN-FRC beam is modeled with 10-node Tetrahedral (Tet) solid elements while anchor and the steel plate are modeled with 8-node Hexahedral (Hex) solid elements with reduced integration, in Abaqus. The analyses are performed by applying a displacement rate on the steel plate in the positive y-direction (see Figure 10). This is done at the level of the concrete upper surface to minimize eccentric effects under the physical tests. Since the analyses shall simulate a static loading scenario but in Abaqus/Explicit are performed dynamically, the load rate is consistent 300 lb per step throughout all numerical simulations. This rate keeps the analysis times to a minimum without adding dynamic effects. The displacement output information is registered throughout the analyses on the Anchor rod, i.e., at the same location as the potentiometer in the physical test (see Figure 11).

4.2 SYN-FRC Beam Anchorage Modeling in ABAQUS

4.2.1 Creating Parts

The first step in ABAQUS is using the “Create Part” tool to model the geometry and regions of a fiber-reinforced concrete anchorage beam. This tool model the dimensions and components for each part, as seen in Figure 14. ABAQUS interface creates the part on a coordinate grid, so the lines refer to the coordinate points. If a portion of the member needs to be cut or perforated, the “Create: Cut Extrude” tool is used.

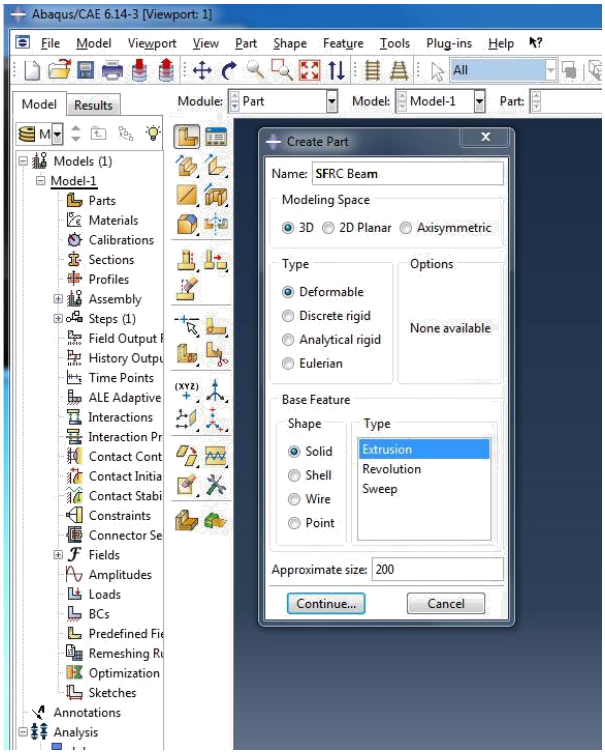

Figure 14. ABAQUS- Initial Step "Create Part"

For this study, the SYN-FRC beam, Anchor rods, and Steel plate are initially individual “Parts” in ABAQUS and then combine to form the SYN-FRC beam anchorage. The process starts with modeling the SYN-FRC component as a rectangular beam, then modeling the second component as steel Anchor rod and the third component as Steel plate. The dimensions of the SYN-FRC beam are 18 inches in depth, 24 inches in height, with a span of 54 inches. The steel Anchor rod is 3/4th inches in diameter with a total length of 10 inches and an embedded length of 6 inches. The dimensions of the Steel plate are 6 inches in width, 16 inches in depth, and 1 inch in thickness. The solid extrusion for the Steel plate hole is slightly bigger than the diameter of the Anchor rod to accommodate the connection. Following AISC Steel manual for connection design, the hole diameter is 1/8th inch bigger than the Anchor rod of 3/4th inch diameter. These dimensions come from the SYN-FRC beam in the available experiment, as seen in Figure 15-16. A summary of the measurements for each component can be seen in Table 9. Modeling of each SYN-FRC beam part before assembling is shown in Figures 17-19.

Table 8. Dimensions of SYN-FRC beam, Steel Plate and Anchor rod

SYN-FRC Beam			
Length (in.)	Height (in.)		Depth (in.)
54	24		18
Anchor rod			
Diameter (in.)	Total Length (in.)		Embedded Length (in.)
0.75	10		6
Steel Plate			
Width (in.)	Height (in.)	Hole Diameter (in.)	Thickness (in.)
6	16	0.875	1

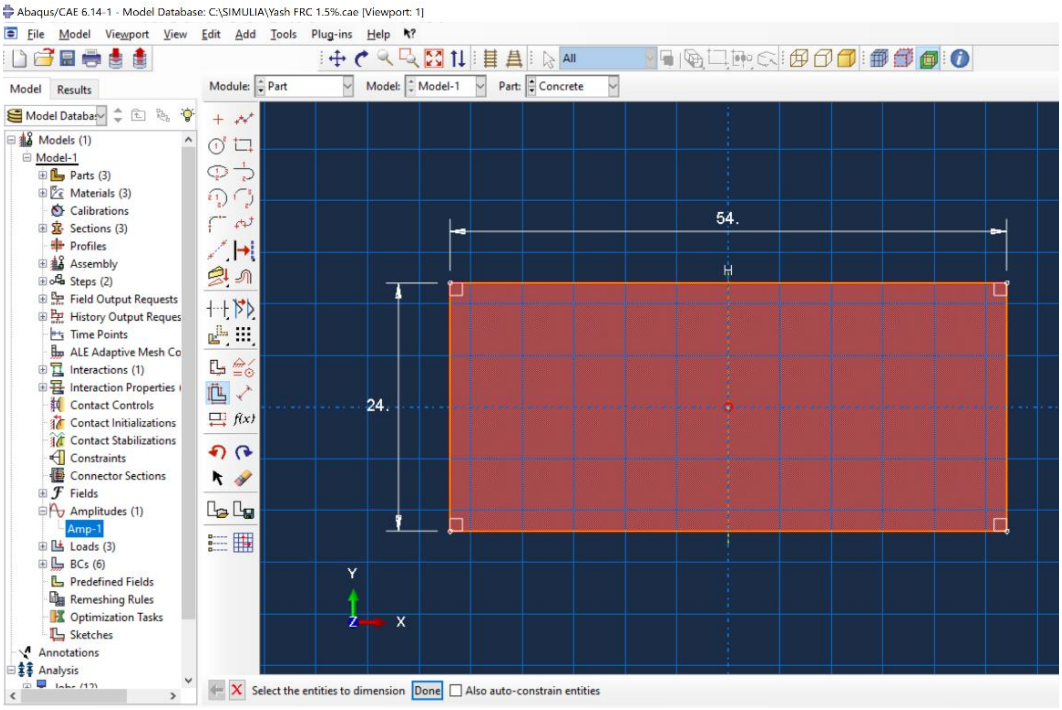

Figure 15. ABAQUS SYN-FRC Beam Cross Section (Units are inches)

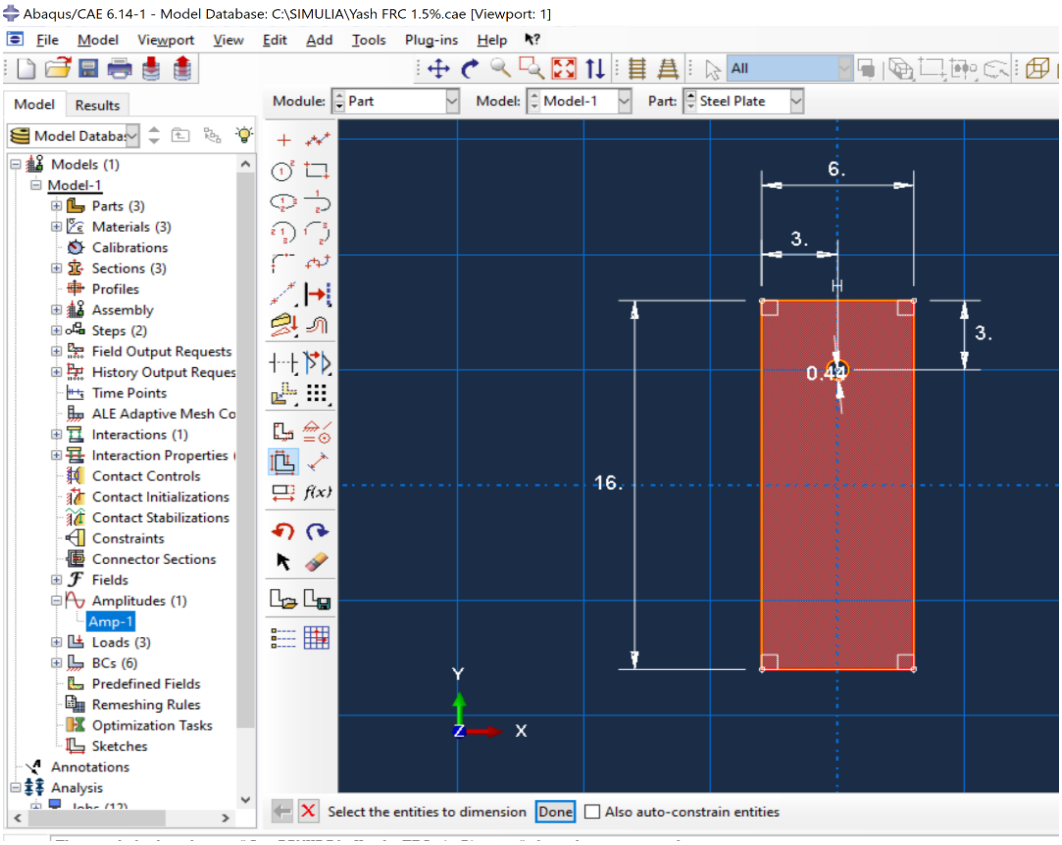

Figure 16. ABAQUS-Steel Plate Cross-Section (Units are inches)

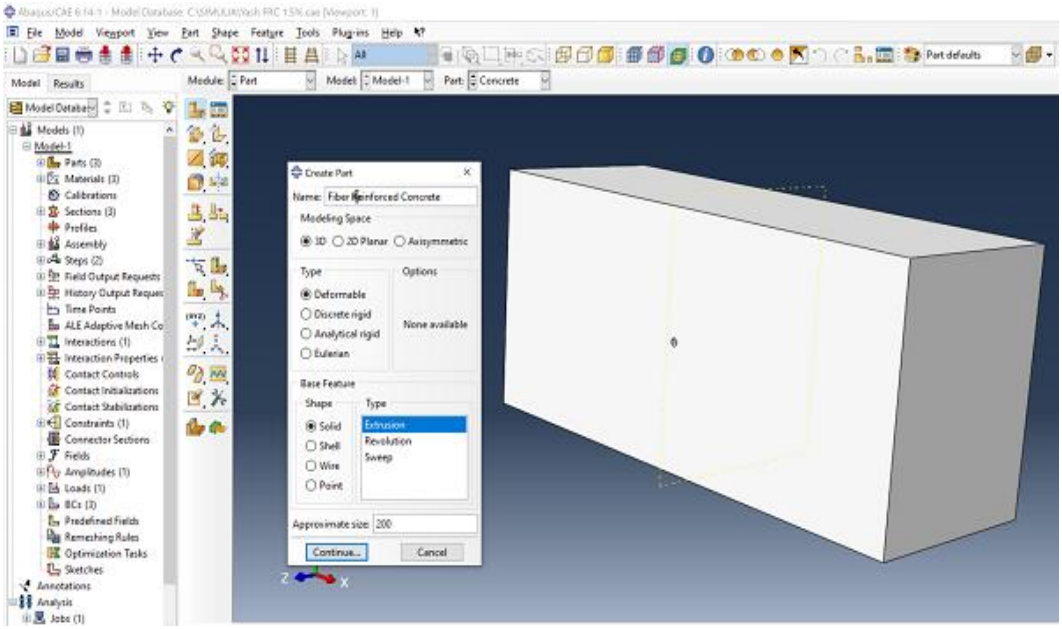

Figure 17. SYN-FRC Solid Shape

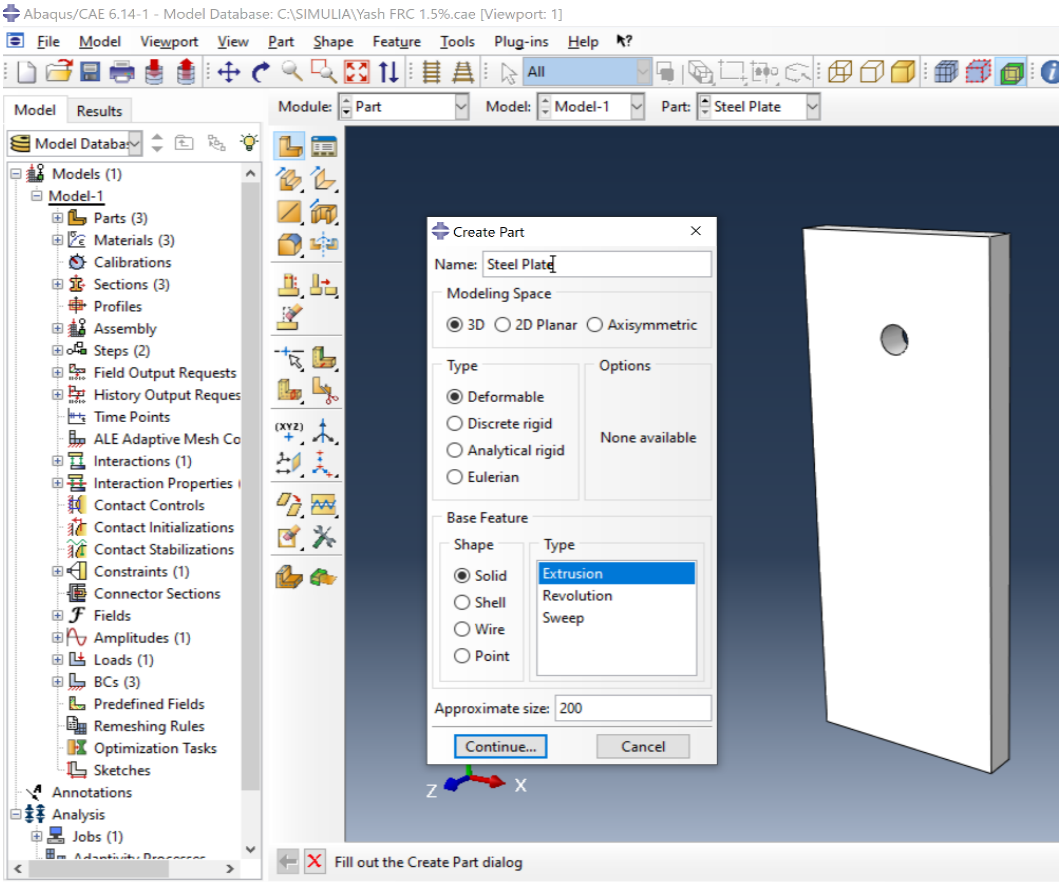

Figure 18. Steel Plate Solid Shape

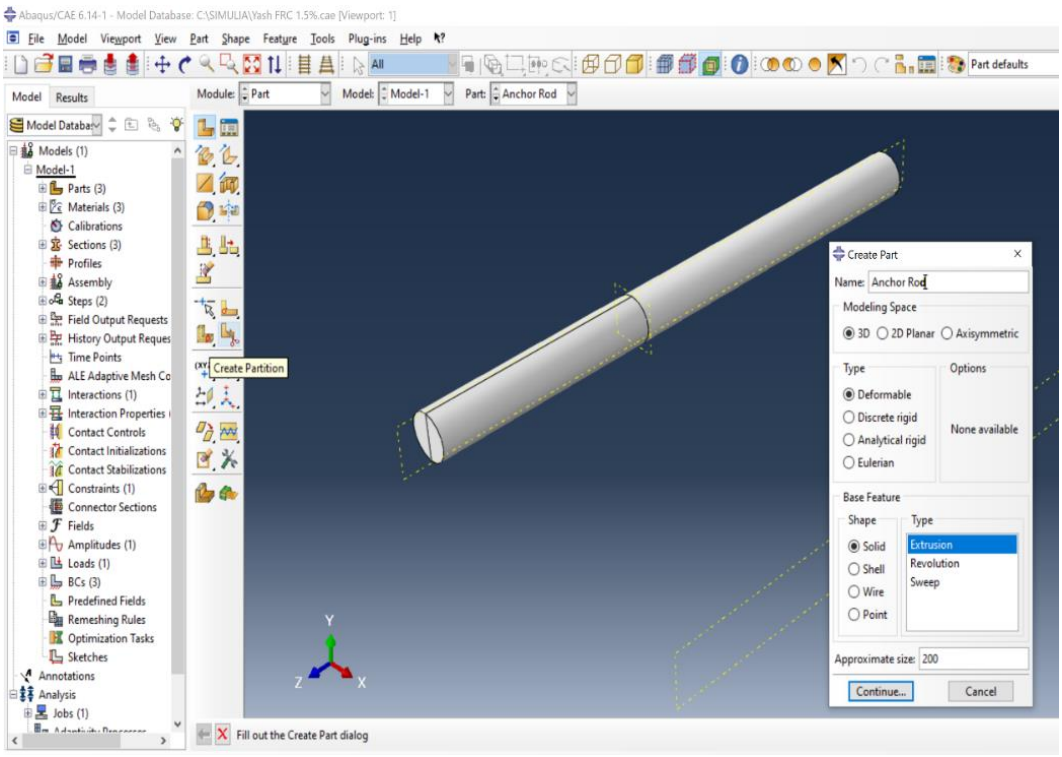

Figure 19. Anchor rod Solid Shape

4.2.2 Material Properties

The strength properties for the Experiment Specimen are put into ABAQUS. For Finite Element Analysis (FEA) for the model, the physical properties of the individual parts must be input into the “Material Manager” tool, as shown in Figure 20. This tool defines the materials, sections, and assigns section to the parts. The mass density for each material is obtained by multiplying bulk density with a slug conversion factor (0.0031).

Different properties are given for the parametric studies to determine the impact that Polypropylene fiber percentage can have on a SYN-FRC anchorage. Values from the material properties tests, precisely the compressive strength (fc’), tensile strength (ft’), and Modulus of rupture (fr’), are input into ABAQUS for each case. The Elastic Modulus (E) is adjusted for each case, which changes according to the percent of polypropylene fibers, as seen in Table 10. The computation of E for the numerical analysis is shown in the parametric study of this research in chapter 5. The parameters and other physical properties input into ABAQUS can be seen in Tables 9, 10, and 11.

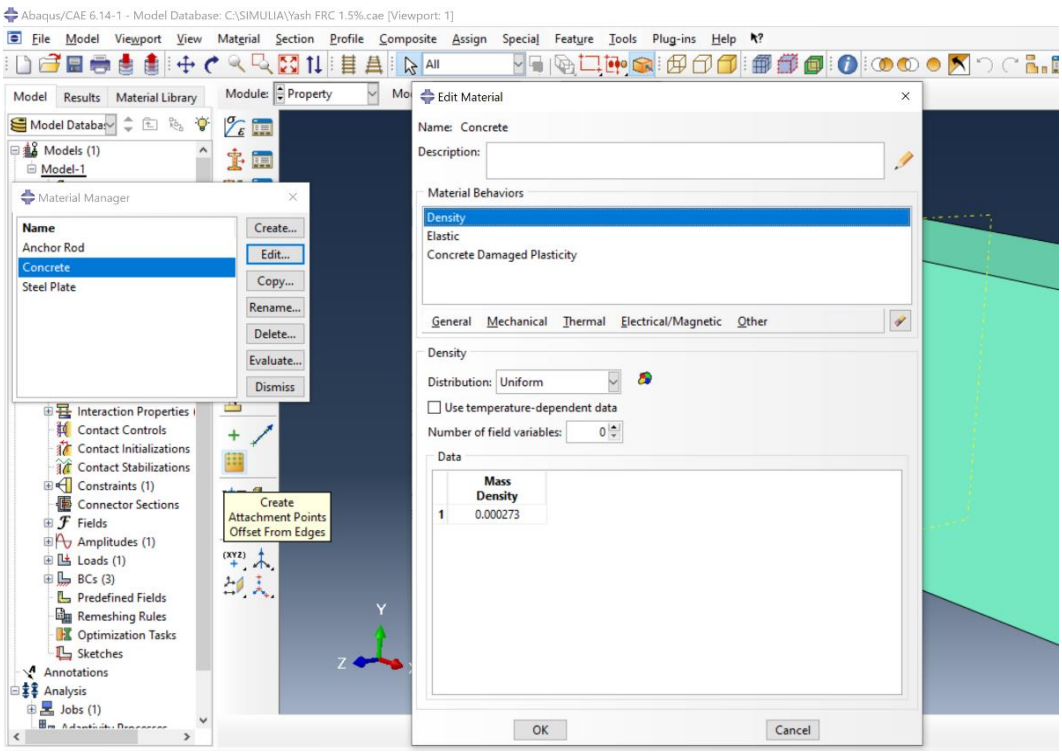

Figure 20. ABAQUS-Material Edit Tool

Table 9. Material Properties of Analyzed SYN-FRC Specimens

FRC Parametric Study Parameters (PSP)				
Fiber Volume Fraction (%)	0%	0.50%	1.00%	1.50%
Compressive strength (psi)	3637	3377	2942	2750
Tensile Strength (psi) (Khanfar M. et al. 2019)	135.3	163.8	195.1	214
Modulus Rupture (psi) (Khanfar M. et al. 2019)	412.4	477.7	536.6	653.2
Elastic Modulus (psi)	3437530.07	3405128.46	3246276.36	3141549.586

Table 10. Material Properties of Analyze Steel Plate Specimen

Steel Plate (ASTM A514 Grade B)	
Yield Stress (ksi)	100
Elastic Modulus (ksi)	29000
Bulk Modulus (ksi)	20300
Shear Modulus (ksi)	11600
Poisson's Ratio	0.3

Table 11. Material Properties of Analyzed Anchor Specimen

Steel Anchor Bolt (F1554 G105)	
Yield Stress (ksi)	60
Elastic Modulus (ksi)	29000
Poisson's Ratio	0.3

4.2.3 Concrete Damage Plasticity

The concrete damaged plasticity model (CDP) is based on work carried out by (Lee et al. 1998) and (Lubliner et al. 1989) and is available in both the implicit and the explicit integration solver (Abaqus/Standard and Abaqus/Explicit). The CDP model uses the concept of isotropic damaged Elasticity in combination with isotropic tensile and compressive plasticity to represent the Elastic behavior of concrete. The model consists of the combination of non-associated multi-hardening plasticity and scalar (isotropic) damaged Elasticity to describe the irreversible damage that occurs during the fracturing process.

The model allows the definition of strain hardening in compression and can be defined to be sensitive to the straining rate, which resembles the behavior of concrete more realistically.

Parameter	Description	Default value
ψ	Dilation angle	User defined
ϵ	Flow potential eccentricity	0.1
σ_{b0}/σ_{c0}	Ratio of initial equibiaxial compressive yield stress to initial uniaxial compressive yield stress	1.16
K_c	Ratio of the second stress invariant on the tensile meridian to that on the compressive meridian at initial yield for any given value of the pressure invariant such that the maximum principal stress is negative	0.6667
μ	Viscosity parameter	0.0 in Abaqus/Standard N/A in Abaqus/Explicit

Figure 21. ABAQUS-Concrete Damage Plasticity (Dassault Systémes 2010)

The CDP model assumes non-associated potential plastic flow in which the Drucker-Prager hyperbolic function describes the flow potential G [Dassault Systémes 2010].

$$G = \sqrt{(\in \cdot \sigma_{t0} \cdot tan\psi)^2 + \bar{q}^2} - \bar{p} \cdot tan\psi \quad \text{.....(6)}$$

In the equation, $\bar{q}$ denotes effective Mises stress, and p denotes the effective stress caused by hydrostatic pressure. The dilation angle ψ is measured in the p-q plane at high confining pressure and indicates the ratio between the volume change and the shear strain. The dilation angle value for concrete is commonly specified in the range of 30° to 40°. The flow of potential eccentricity defines the rate at which the function approaches the asymptote. With the default value of 0.1, the dilation angle is almost the same over a wide range of confining pressure stress values. The uniaxial failure tensile stress σt0 is via the tension stiffening definition specified by the user (Dassault Systémes 2010).

Table 12. Concrete Damage Plasticity Parameters

Dilation Angle	Eccentricity	fb0/fc0	K	Viscosity Parameter
31	0.1	1.16	0.667	0

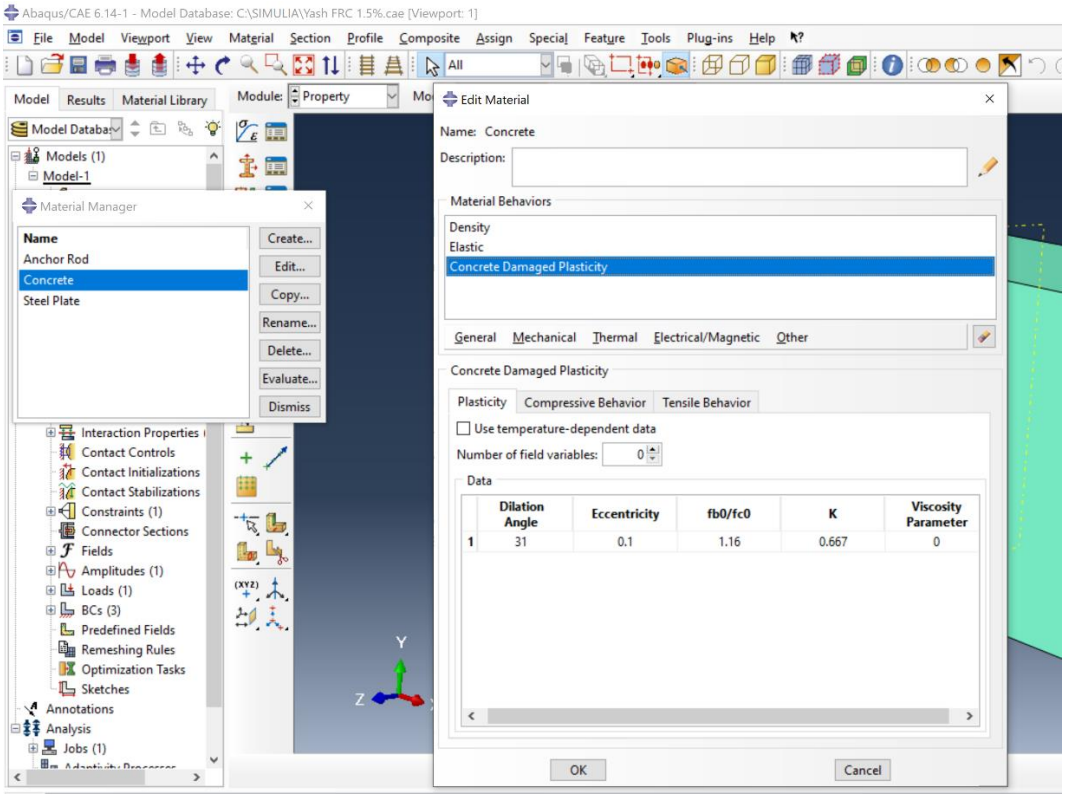

Figure 22. ABAQUS-Concrete Damage Plasticity

4.3 Assembly of Components

After modeling the parts and assigning the properties, the “Assembly” tool combines each element to form the test set up, as shown in Figure 23. The Anchor rods are embedded into the SYN-FRC beam in the same manner for each study. Embedding the members prevents two material from overlapping the member that ABAQUS analyzes and still maintain the input properties for each one. The Steel plate is attached for the transfer of shear force.

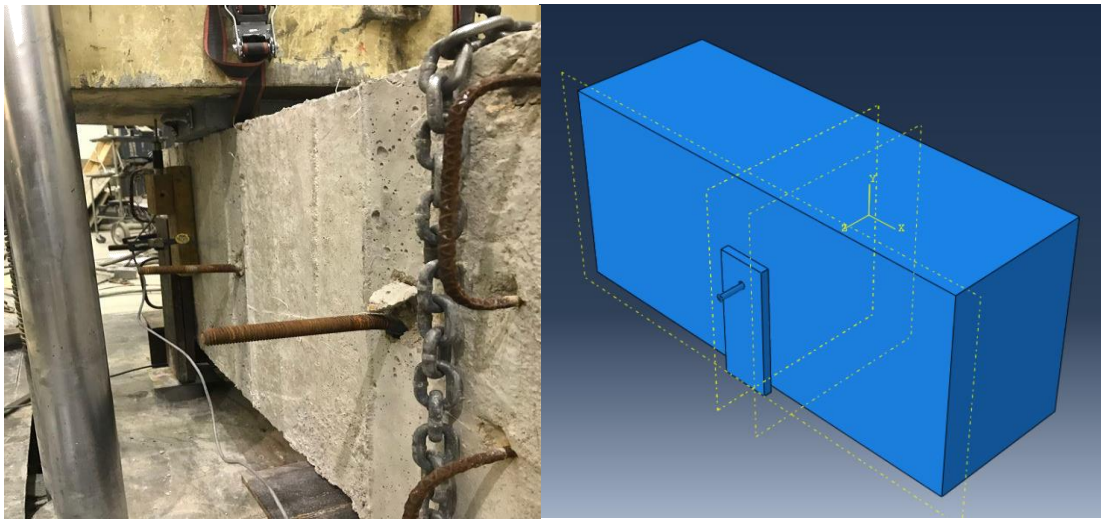

(a) (b)

Figure 23. (a) Experimental set up (Khanfar M. et al. 2019) (b) ABAQUS-Assembly of SYN-FRC and Angle Steel

4.4 Steps and Time Increments

The step tool defines each analysis step and the output requests for the ABAQUS model. Each step is created and used for the loading process, as shown in Figure 24. In this study, each step an additional load was added onto the beam to imitate the monotonic loading process used by an actuator in an actual experiment. When creating the step, each one has a set increment, which can steadily increase the load up to the point of collapse in 100 smaller steps. This is the automatic setting in ABAQUS, as seen in Figure 25.

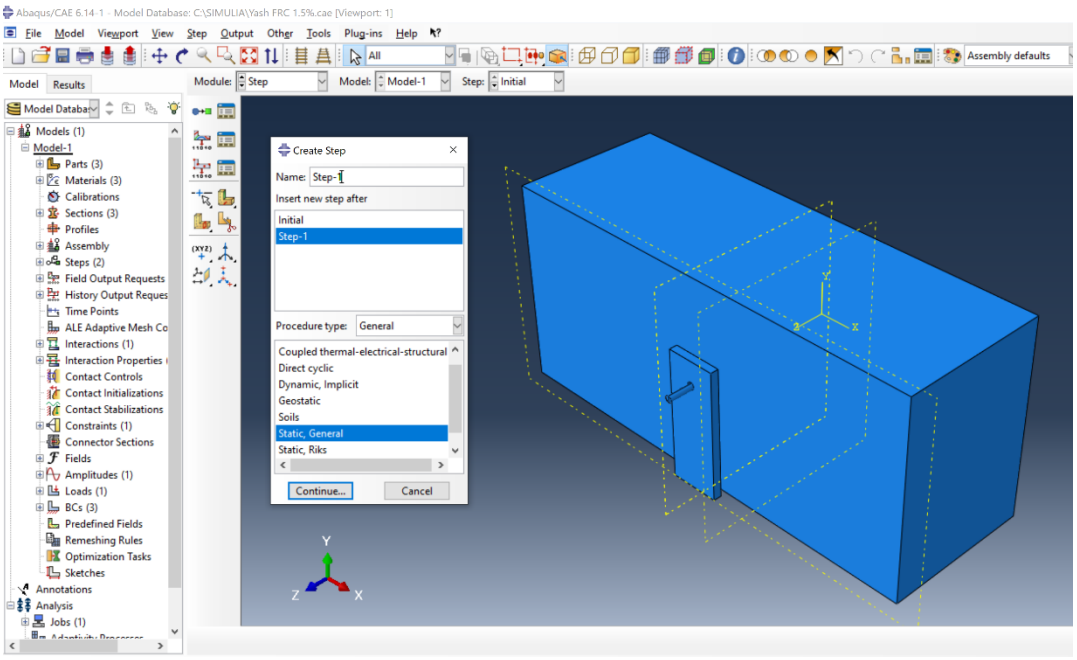

Figure 24. Create Step for each Load

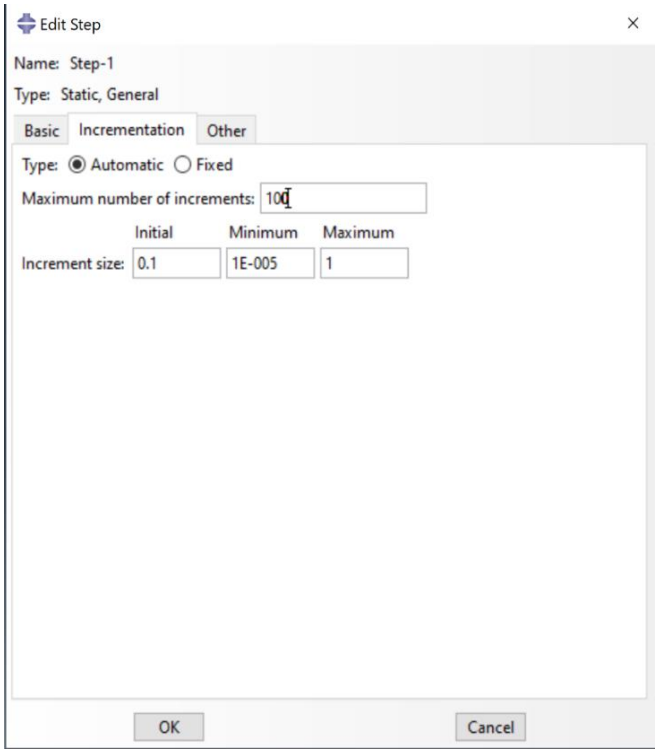

Figure 25. Increments of 100 per Step

4.5 Interaction and Constraints

The interaction of the steel plate to the Anchor rod is crucial as in the experiment, the steel plate is held to the Anchor rod by fastening with a nut. There is a friction plane interacting between the inner surface of the hole in the steel plate and the outer surface of the Anchor rod. Figure 26 shows the surface interaction modeling in ABAQUS. C3D10 are textbook formulation second-order tetrahedral elements. Upon applying a uniform pressure load to the face of these finite elements, it generates zero nodal forces at the corner node rendering them not suitable for contact simulations. This drawback could be negated with the usage of a finite sliding surface to the surface formulation for contact. ABAQUS recommends using this combination for any contact analysis with C3D10 tetrahedral elements. Here enforcement method also plays a crucial role. C3D10 elements are recommended for any contact involving finite sliding with node to surface or surface to the surface formulation when used with a penalty enforcement method. For this model, the surface to surface interaction is adopted.

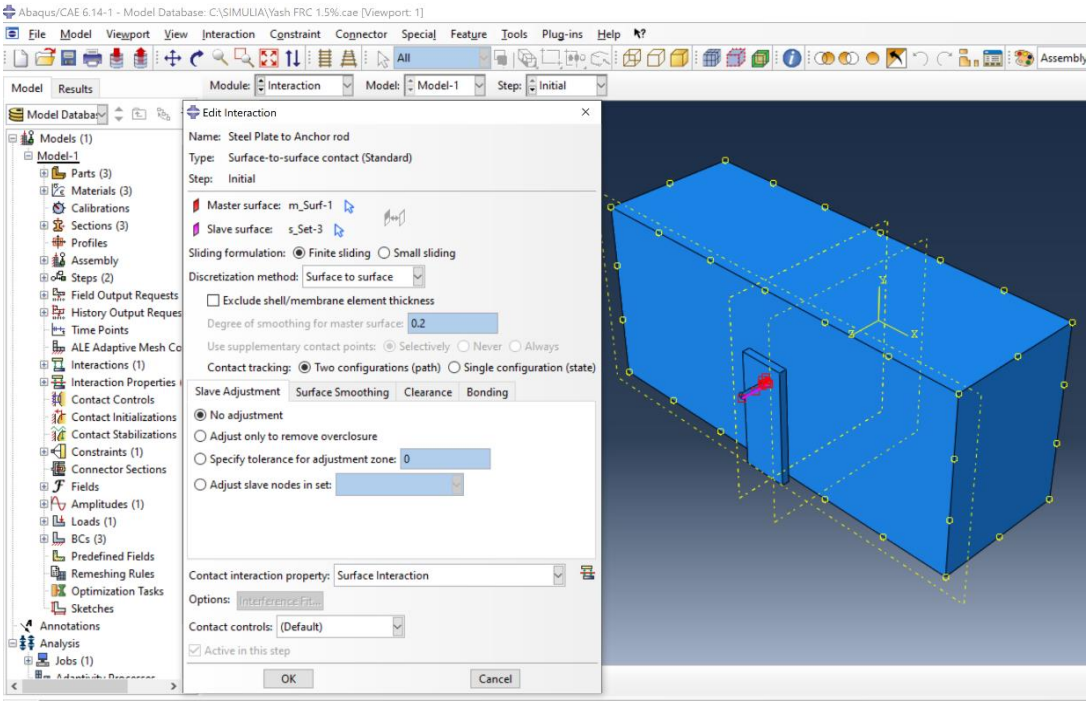

Figure 26. Surface to surface interaction between Steel plate and Anchor rod

It is essential to showcase the Anchor rod as an embedded region in the SYN-FRC beam. This constraint can be achieved by modeling the embedded surface of the Anchor rod as a slave surface while the entire SYN-FRC beam was acting as a host body, as shown in Figure 27. It is important to model in such a manner because at the time of analysis, the software needs to identify the type of material, and only then can it show deflection and stresses in a material. Otherwise, the software overlaps two material and could not identify the kind of material failure.

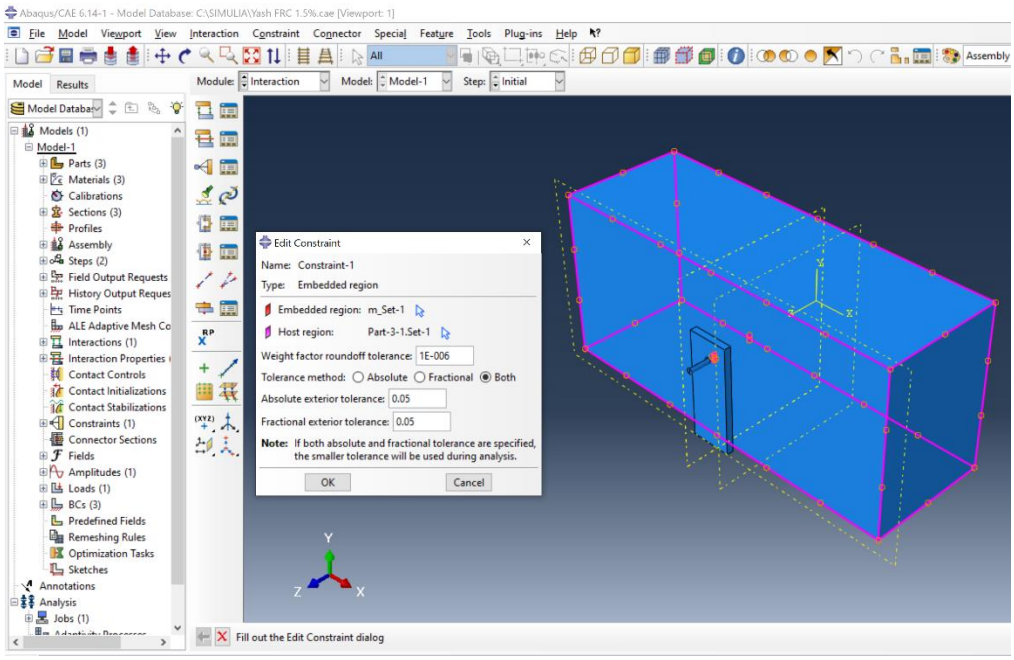

Figure 27. Anchor rod embedment into the SYN-FRC beam

4.6 Loads and Boundary Conditions

A Load is made using the “Create Load” tool, as seen in Figure 28 (a). For each step, the load act in an upward direction. This is to observe the Anchor rod and concrete behavior in shear and upward displacement like the available experiment, as shown in Figure 28 (b). Loads increase with each step at a rate of 300 lb per step till the anchor bends or ruptures. The load-step can be adjusted, as shown in Figures 29. The load is applied as an amplitude of magnitude one since the load is applied in positive Y-direction (upward). The increment of the load is 300lb with each step, and Figure 29 shows the amplitude table.

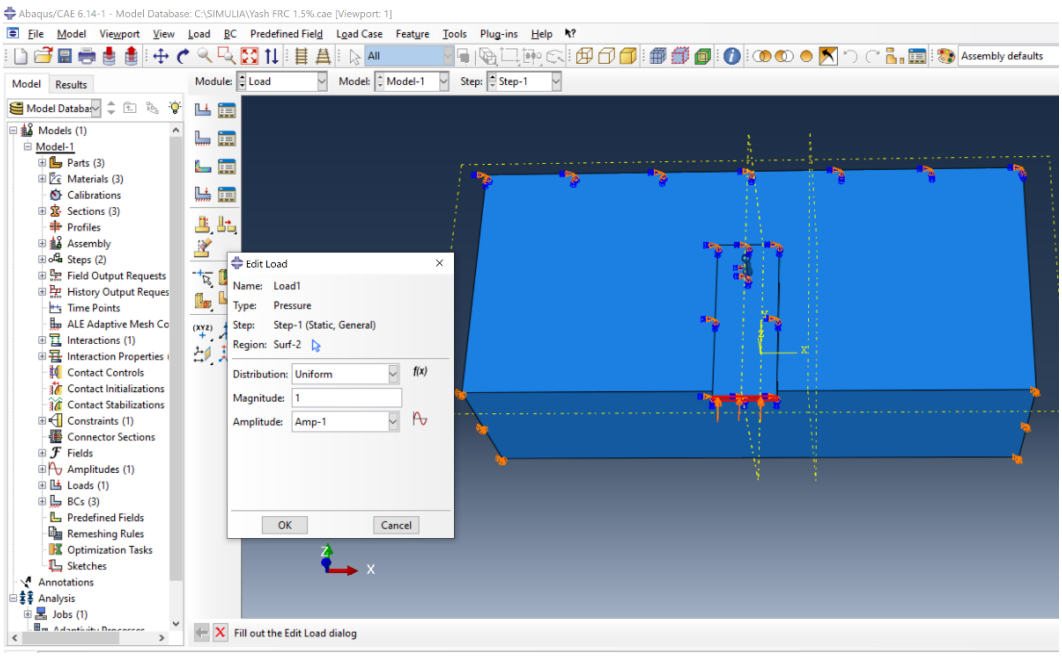

(a)

(b)

Figure 28. (a) Create a Load for each Step (b) Loading in the experimental setup (Khanfar M. et al. 2019)

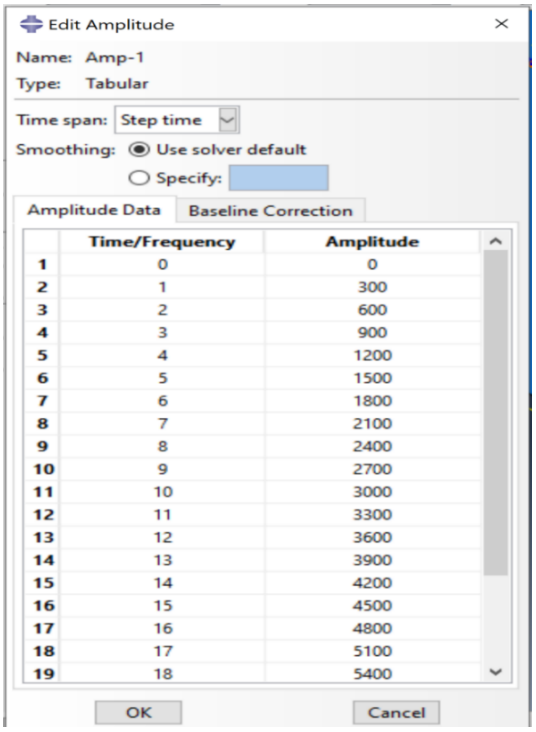

Figure 29. Step time loading at 300lb/sec

Figures 30-33 show the modeling steps for the Boundary Conditions (B.C.) for each element and assembly together. For the model to deliver results commensurable to the experimental results, boundary conditions should be set right. The “Create Boundary Condition” tool allows the user to set the values for the displacement at each DOF.

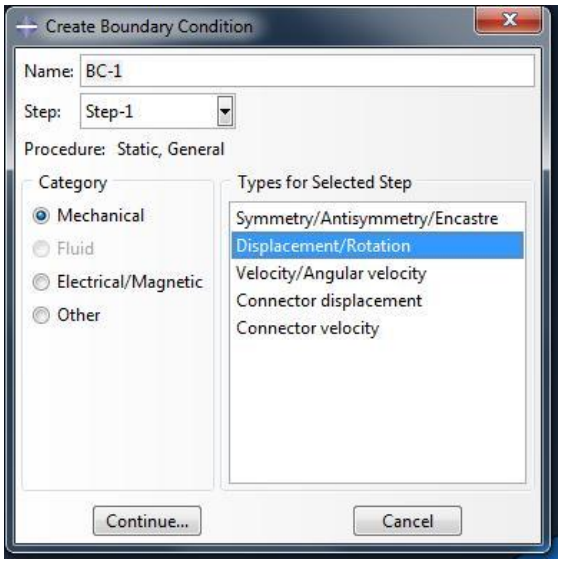

Figure 30. Boundary Condition (B.C.) – Displacement/Rotation

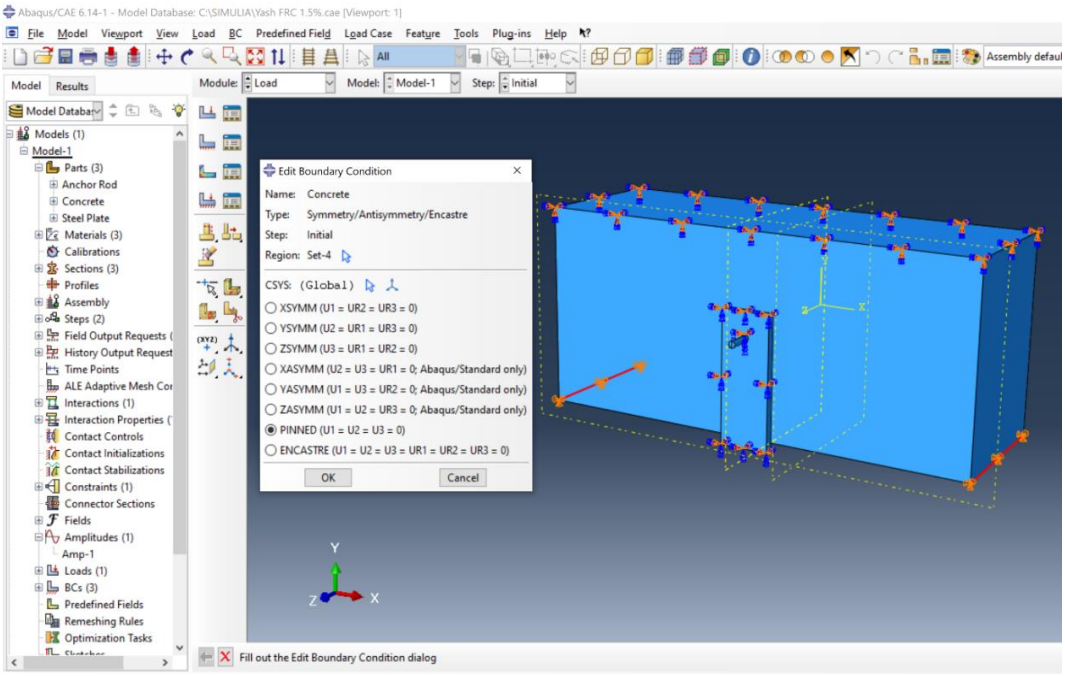

Figure 31. B.C. set as pinned for simply supported concrete

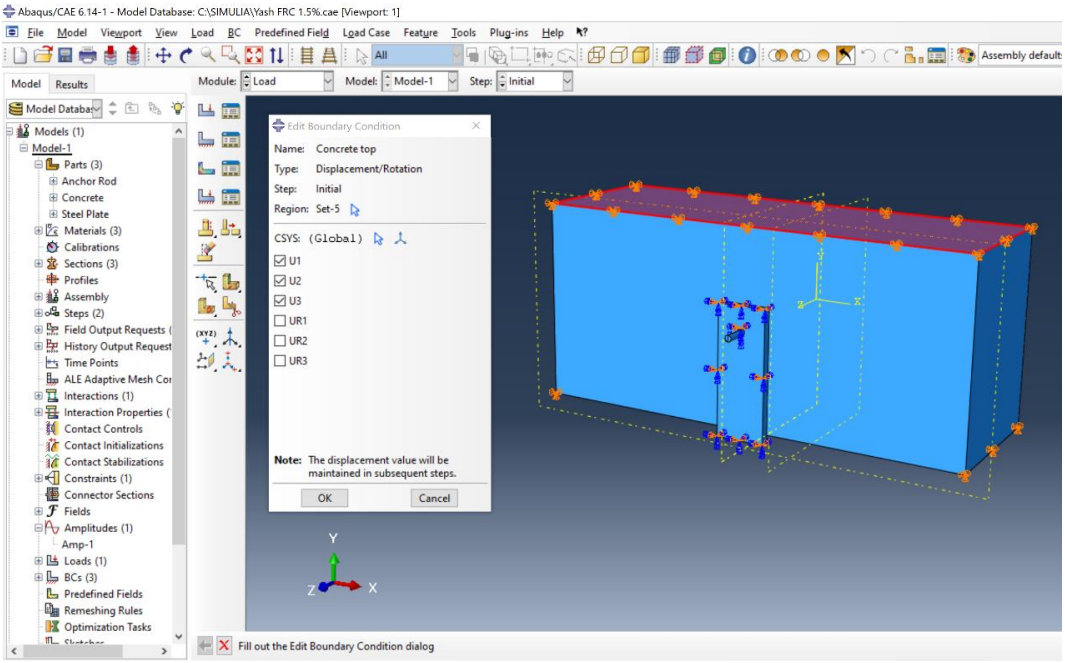

Figure 32. B.C. set for concrete top

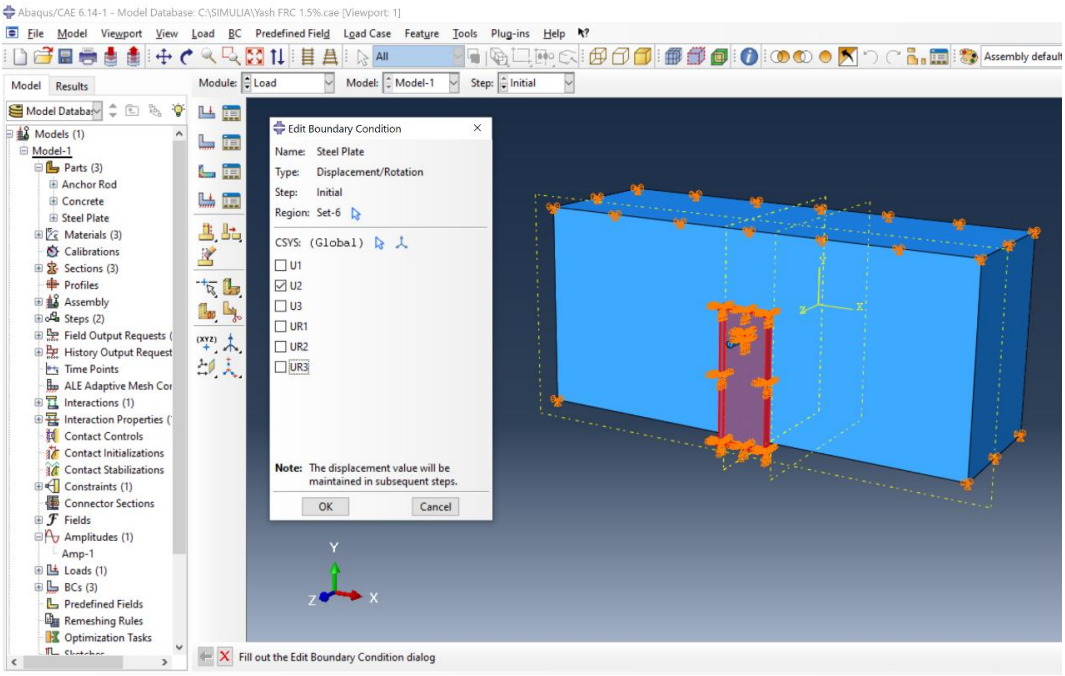

Figure 33. B.C. set for steel plate

4.7 Meshing Components

The SYN-FRC beam is modeled with 10-node C3D10 Tetrahedral (Tet) solid elements while anchor and the steel plate are modeled with 8-node Hexahedral (Hex) solid elements with reduced integration, in Abaqus. C3D10 are textbook formulated second-order tetrahedral elements used for the analysis of small-displacement near the Anchor rod and concrete interphase. A mesh is created on the SYN-FRC beam to discretize the model and form nodes on the components where the displacement develops. Refining the mesh gives more degrees of freedom as more elements are created in the critical areas where stress occurs while a coarse mesh should be designed in general areas where there is not a high amount of stress. When doing a refined mesh, the region can sometimes fail. Some of the reasons may be “inadequate seeding” or “bad geometry”. In this case, the steel Anchor rod has small edges and faces that make the instance imprecise. ABAQUS recognizes this as a wrong geometry, and the assembly needs to have meshed as a tetrahedral (Tet elements) instead of hexahedral (cubic elements) when choosing a refined mesh. Figure 34-35 shows the meshed finite element model.

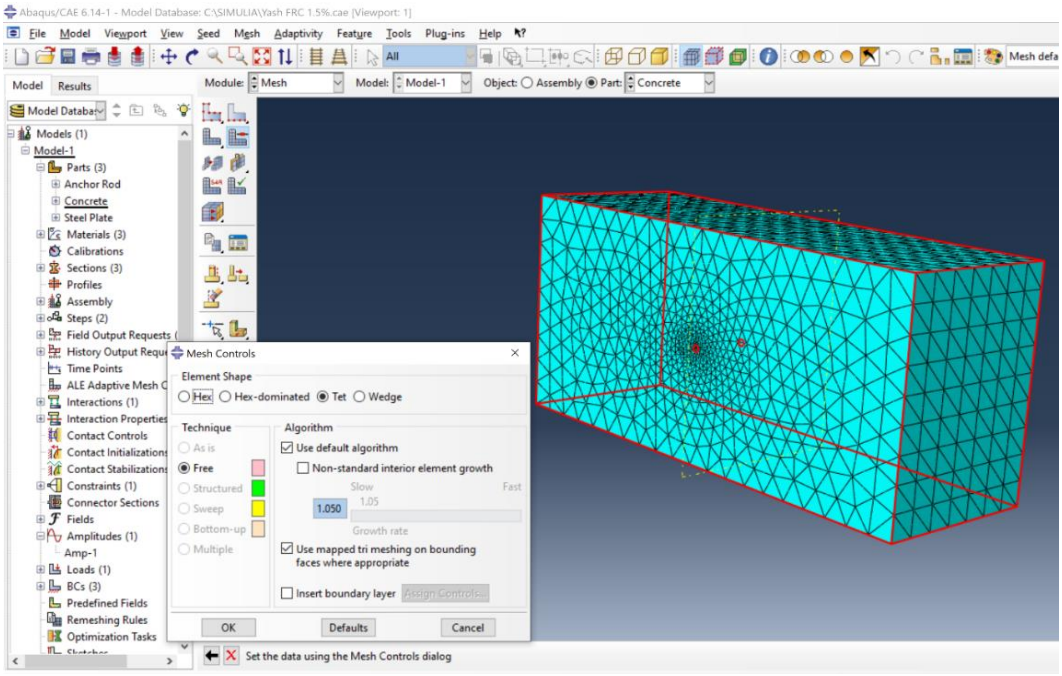

Figure 34. Tetrahedral (Tet) mesh for Fiber Reinforced Concrete

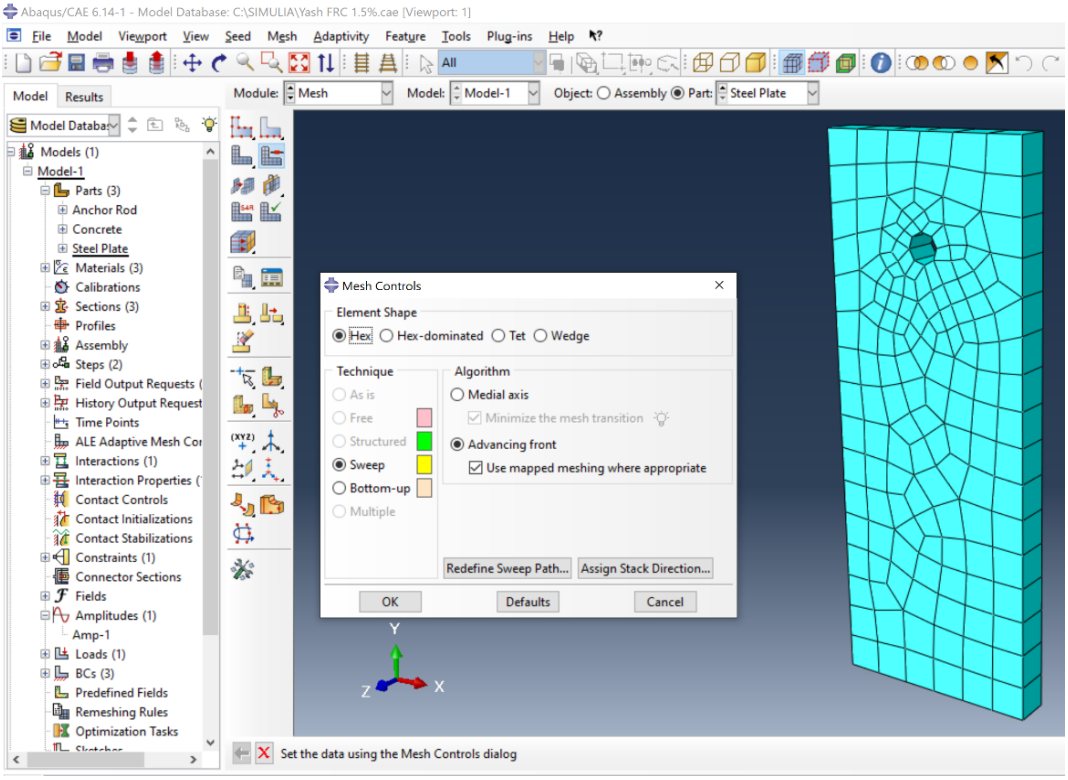

(a)

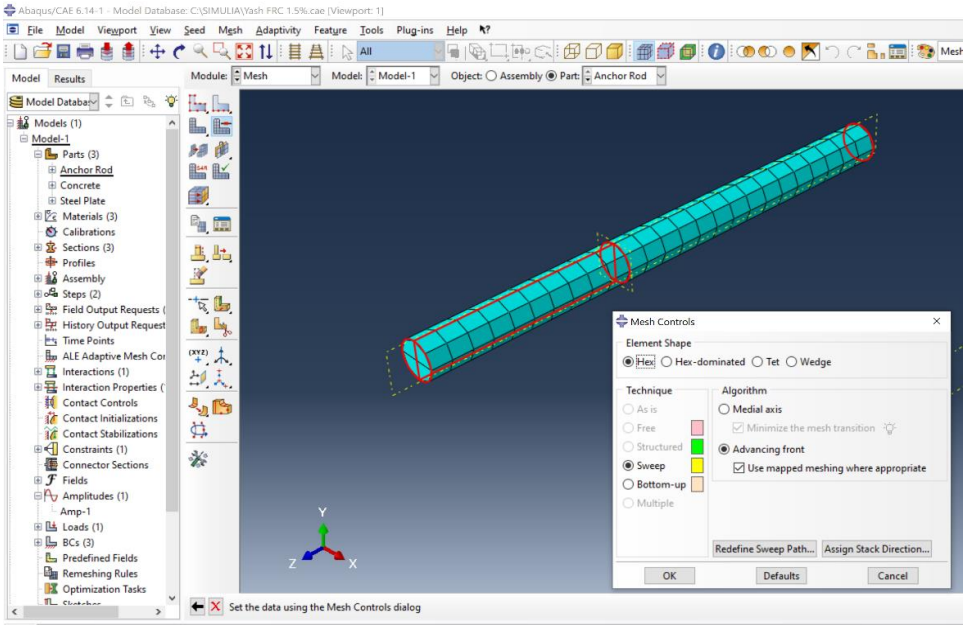

(b)

Figure 35. (a) Hex mesh for Steel plate (b) Hex mesh for Anchor rod

4.8 3D Visualization

After the job is complete in ABAQUS, the interface allows the user to visualize the results in a 3D display, as shown in Figure 36. The regions in the model have different shades of colors to show the distribution of stress and displacement.

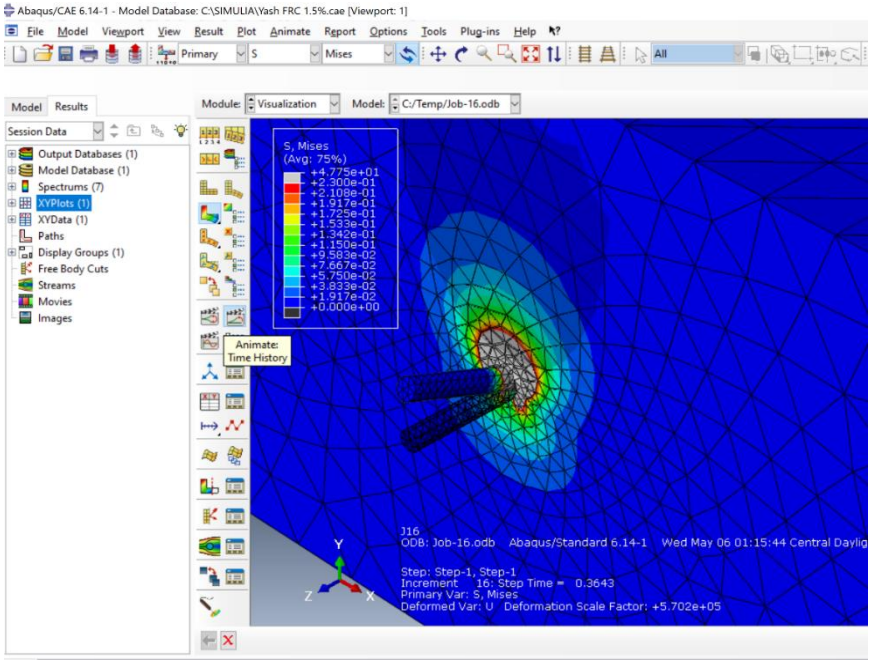

Figure 36. 3D Visualization of Results

Chapter 5

NUMERICAL ANALYSIS

5.1 General

The concrete serves best for its compressive strength while the fibers are introduced to enhance the tensile strength of concrete. Hence, the combined effect can only be studied by both experimental and numerical analysis. Therefore, the response of mechanically loaded anchors in fiber reinforced concrete structures can only be understood by a combination of testing and numerical simulations. As concrete is a complex material, the interaction between anchors and fiber concrete is consequently also complex. Reported work within this area in the open literature is limited and which is why efforts are needed to fill this gap.

In this research project, the response of cast-in-place anchors in fiber reinforced concrete structures is investigated utilizing finite element simulations. Concrete breakout with a single anchor in shear with various percentage of dosage of polypropylene fibers is studied. However, as most of the available testing is conducted on plain concrete and as codes for design of anchors also are based on plain concrete, simulations in this project cover effects on the concrete breakout strength with anchors in shear within fiber reinforced concrete. Simulations are conducted with the general-purpose finite element program Abaqus. Among three available constitutive models, the concrete damaged plasticity model is found to fit the purpose best. Several parameters are investigated, such as finite element size, the effect of fiber dosage on concrete strength properties, Modulus of Elasticity, and the type of boundary conditions. The effect of all these phenomena is investigated in this work. Higher loads on the anchor group compared to that on the single anchor might result in different conditions in the concrete in the vicinity of the anchors. Thus, with a more flexible concrete structure, the failure mechanism splitting instead of concrete cone breakout might limit the anchor group capacity.

5.2 Mesh Convergence

For determining displacement, a mesh convergence study helps to choose the right number of elements in the SYN-FRC beam. A finer mesh density discretizes the displacement area and the curvature inflection points. A specific geometrical cross-section is designed as the mesh depending on the optimal configuration by ABAQUS. Before performing each study, a mesh convergence study is done to confirm what type and dimension of a mesh can allow for an accurate representation of the results. The following process helps determine the ideal mesh size to achieve a precise picture of the beam's behavior. Note that Figures 37 do not represent the results for this research and only shows how the data converges for different mesh sizes.

The Tetrahedral quality measure for the C3D10 element recommends the volume of tetrahedron divided by the volume of an equilateral tetrahedron with the same circumsphere radius. The size of the element recommended is 0 for degenerated tetrahedron and 1 for the equilateral tetrahedron. It is also recommended that the tetrahedral quality measure is greater than 0.02 (Dassault Systémes 2010).

Figure 37 shows mesh convergence for the ABAQUS model. The geometry with 0.25" x 0.25" creates a too dense model with over 100,000 finite elements. This causes a longer time for the software to process the elements and leads to poor analysis. The values do not display the available experiment results and do not show convergence. The values for 0.5" Tet elements show convergence with results, which represent the available experimental results. The 1" Tet elements mesh size does not display the results accurately.

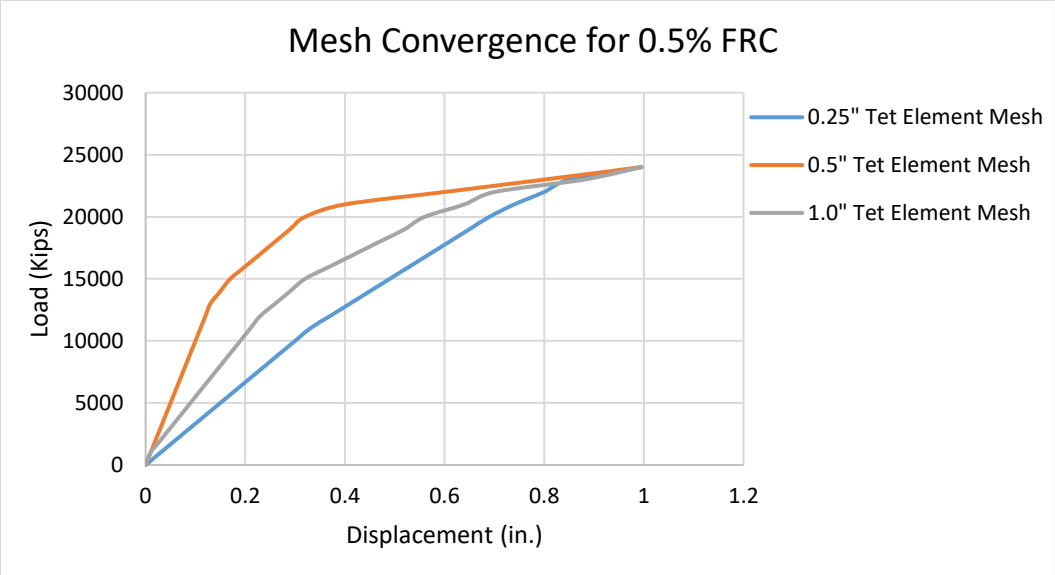

Figure 37. Convergence for 0.5% SYN-FRC Mesh

After analyzing the member with each mesh shown from Figures 37, a mesh of 0.5” Tet Element was chosen. It is most optimal to determine the failure load and displacement for each study. Therefore, 21,819 discrete C3D10 Tet elements experience the load distribution that contributes to various displacement in different regions of the SYN-FRC beam.

5.3 ABAQUS Model Analysis

In the first part of this research, the experiment on a SYN-FRC with cast-in-place Anchor rod is modeled and analyzed. The same properties for the SYN-FRC and specimen dimensions from the available experiment (Khanfar M. et al. 2019) are put into the software. The Model analysis is done with similar load steps as the experimental set-up, and the results are compared to the physical test. Figure 38 shows how ABAQUS displays the shear behavior and stress development of the SYN-FRC beam anchorage.

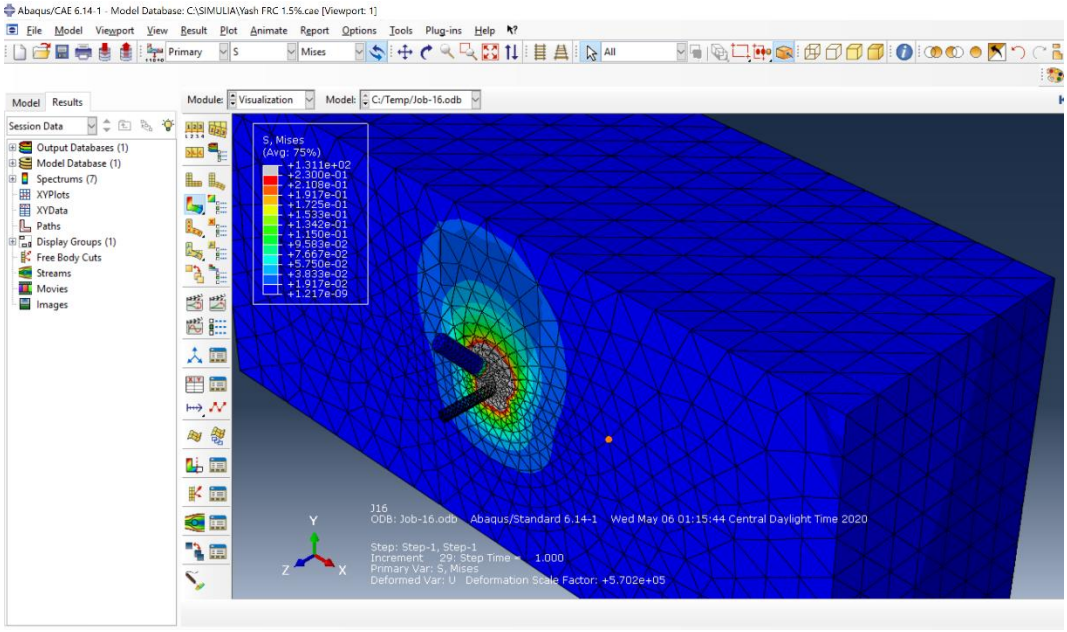

Figure 38. ABAQUS model of Shear behavior of SYN-FRC beam

In FEA, the software shows different regions where the displacement is occurring. The software use interpolation to determine a displacement value over a certain number of elements. From Figure 38, it is observed that the SYN-FRC beam can handle the load, but in the region around the Anchor rod, the beam is experiencing the most amount of deflection. This is the region that is expected to experience the first set of micro cracks. When more load is applied, this region should be the first to fail. The change in the Finite Element model with increasing fiber dosage shows how the deformation and stress concentration in the SYN-FRC beam decreases.

The crack pattern of the available experiment SYN-FRC beam around Anchor rod with different fiber dosage can be seen in Figures 39-46. The ABAQUS model cracking with corresponding fiber dosage is shown in figures as well. The model shows similar stress behavior around the Anchor rod. Figure 40 shows how ABAQUS provides the stresses and displacements occurring around the embedded length of the Anchor rod in the 0% SYN-FRC beam.

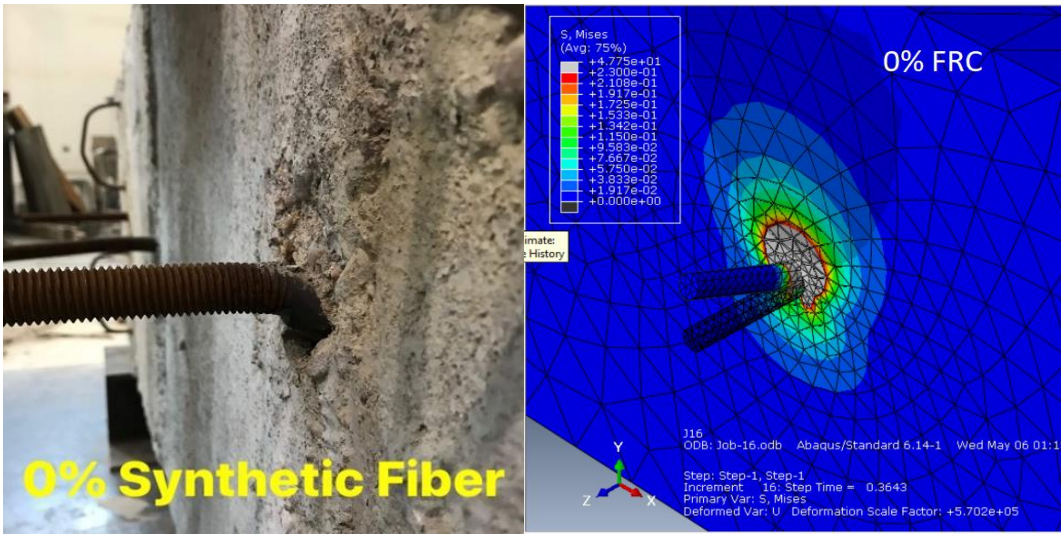

(a) (b)

Figure 39. (a)Experiment test of 0% SYN-FRC Beam (Khanfar M. et al. 2019)

(b) Abaqus Model for 0% SYN-FRC Beam

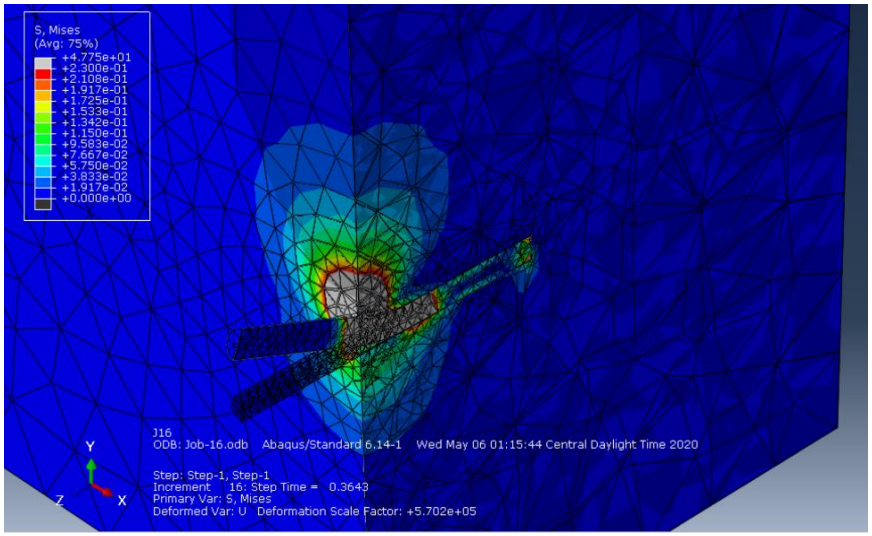

Figure 40. ABAQUS model of Shear behavior of 0% SYN-FRC beam along the embedded length of an Anchor rod

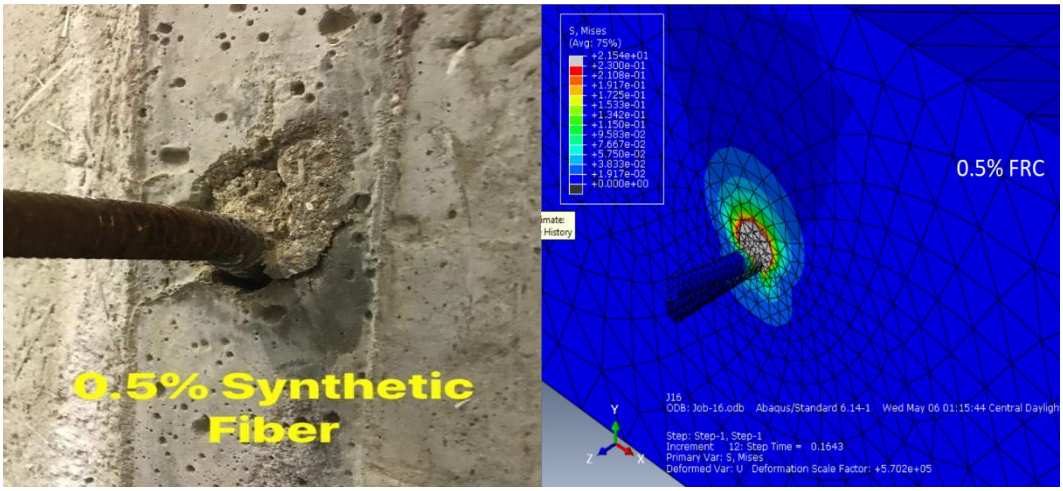

(a) (b)

Figure 41. (a) Experiment test of 0.5% SYN-FRC Beam (Khanfar M. et al. 2019)

(b) Abaqus Model for 0.5% SYN-FRC Beam

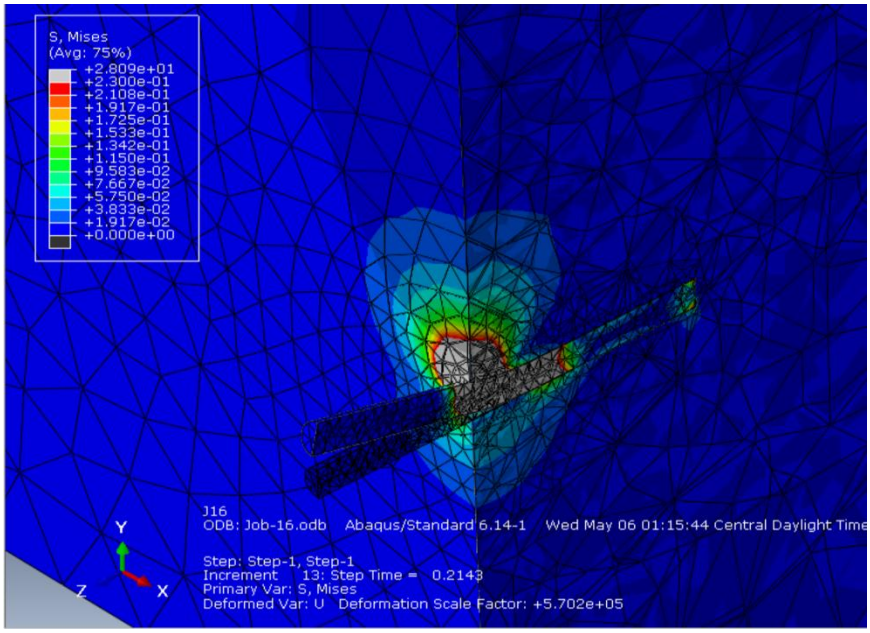

Figure 42. ABAQUS model of Shear behavior of 0.5% SYN-FRC beam along the embedded length of an Anchor rod

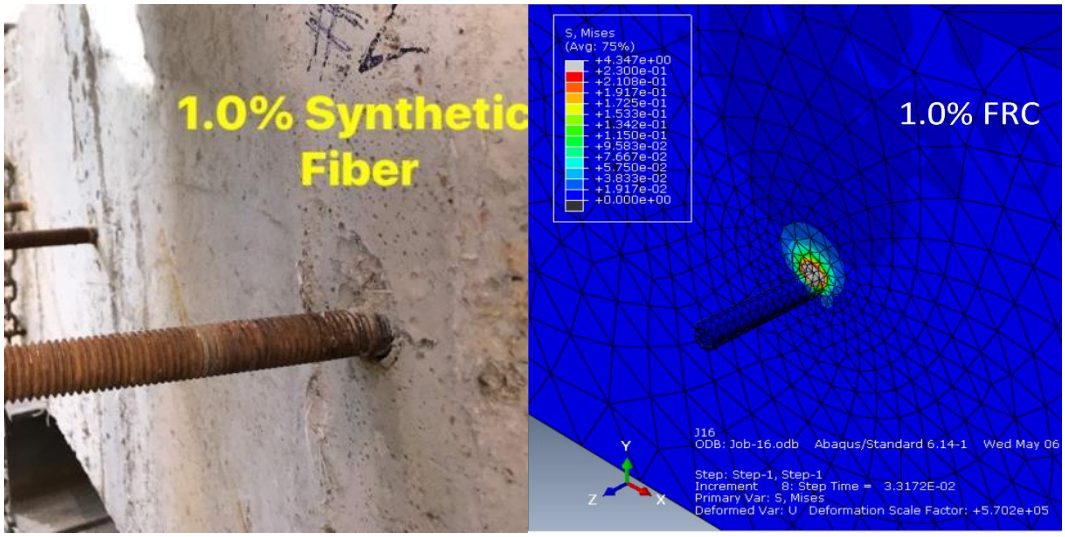

(a) (b)

Figure 43. (a) Experiment test of 1.0% SYN-FRC Beam (Khanfar M. et al. 2019)

(b) Abaqus Model for 1.0% SYN-FRC Beam

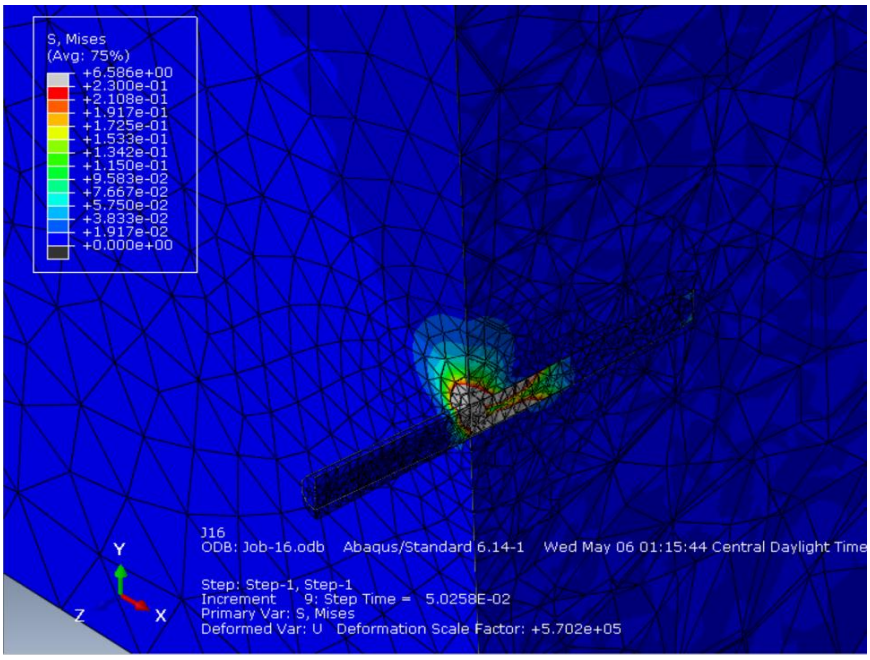

Figure 44. ABAQUS model of Shear behavior of 1.0% SYN-FRC beam along the embedded length of an Anchor rod

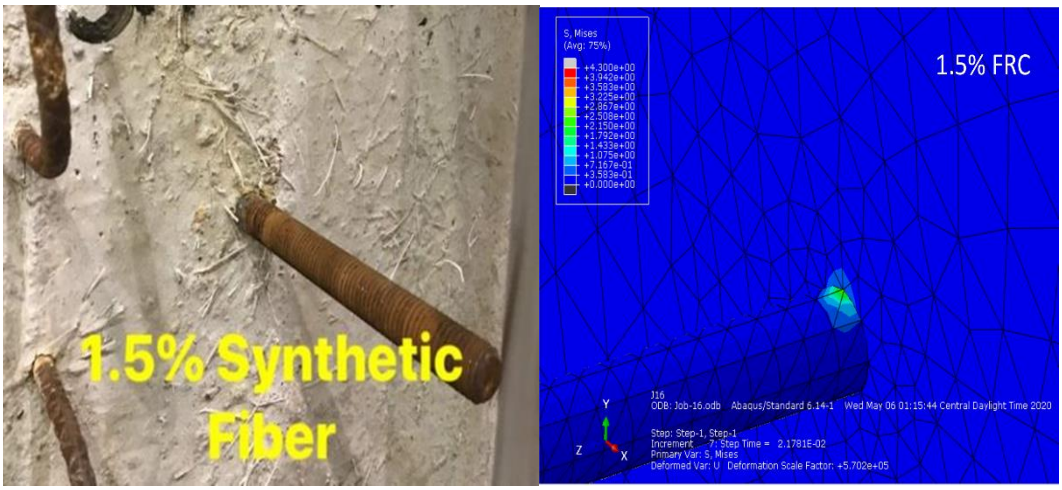

(a) (b)

Figure 45. (a) Experiment test of 1.5% SYN-FRC Beam (Khanfar M. et al. 2019)

(b) Abaqus Model for 1.5% SYN-FRC Beam

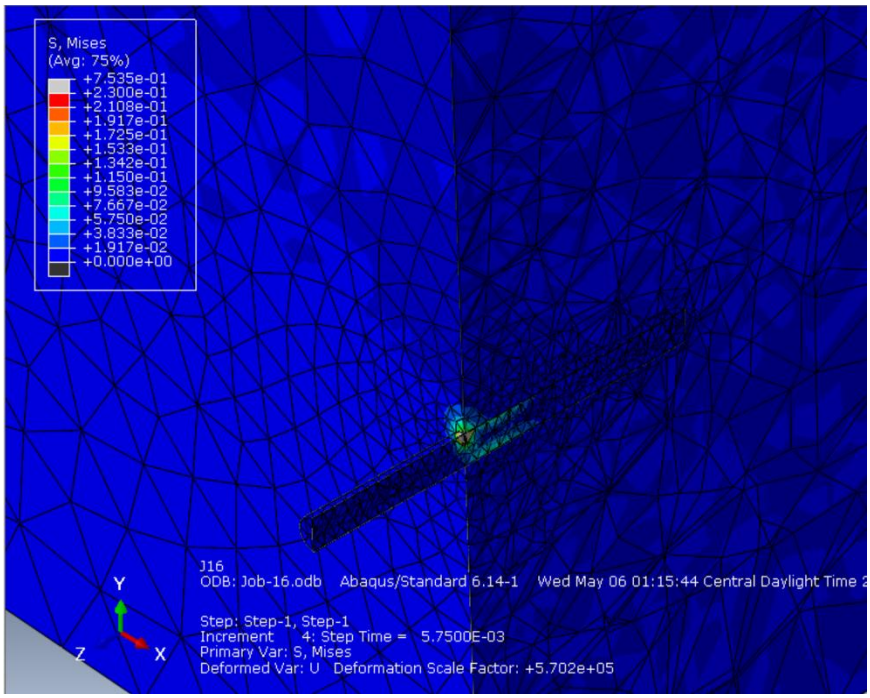

Figure 46. ABAQUS model of Shear behavior of 1.5% SYN-FRC beam along the embedded length of an Anchor rod

It is evident from Figure 39-46 that as the dosage of fiber reinforcement increases, the stress concentration and displacement decreases. It was also observed that the stress reduced along embedment length as the fiber dosage increased within the SYN-FRC beam. One reason for this behavior can be that as the fiber confinement grew around the embedded Anchor rod, the fiber, along with concrete together, resisted the resultant forces developed. It can be advised that with increasing fiber dosage, lesser embedment length can be provided for the similar behavior of SYN-FRC. Although, the stress concentration is also seen at the embedded end of the Anchor rod in the model, and that is why further investigation is required both experimentally and numerically to deduce this conclusion.

Since the model was not designed to mesoscale for the fibers to be randomly distributed in the solid concrete beam matrix, it was important for the model to behave as close as possible with the experimental results. To achieve this, the critical aspect of modeling was to determine the effective Modulus of Elasticity. The empirical formula (Equation 7) to evaluate Modulus of Elasticity underestimates the capacity and hence cannot be used directly. There were several iterations performed with different values of Modulus of Elasticity to calibrate the load-displacement curve. A section was cut to bisect the SYN-FRC beam and the Anchor rod to understand the behavior and forces. Figure 47-50 shows the resultant forces within the model with different dosages of fiber reinforcement.

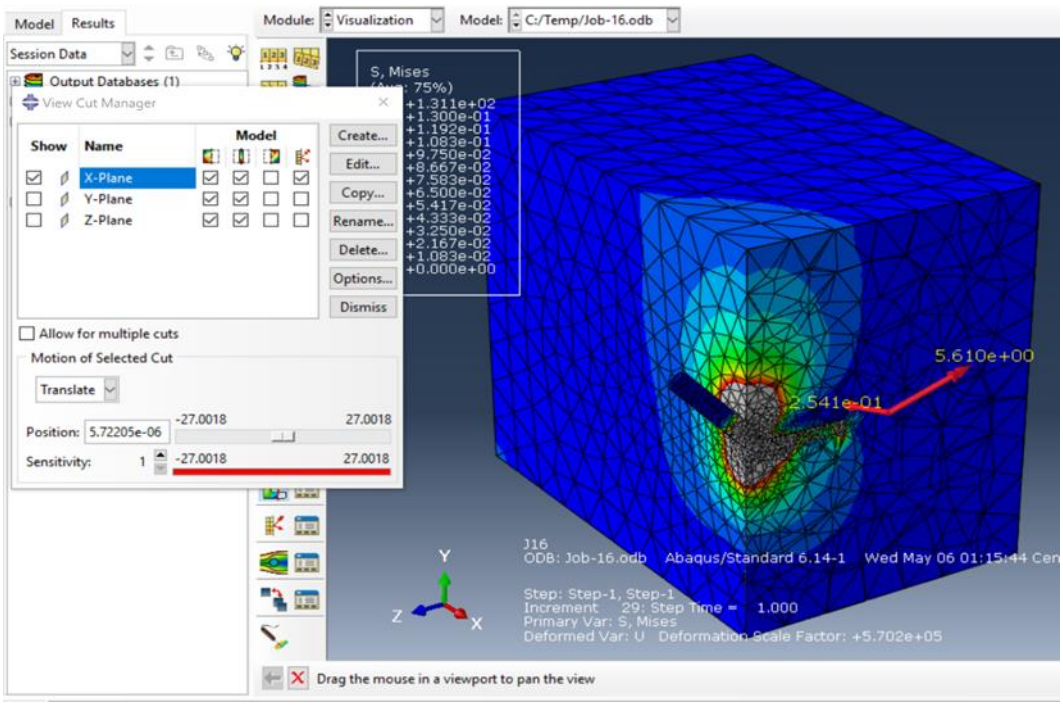

Figure 47. ABAQUS internal force for 0%

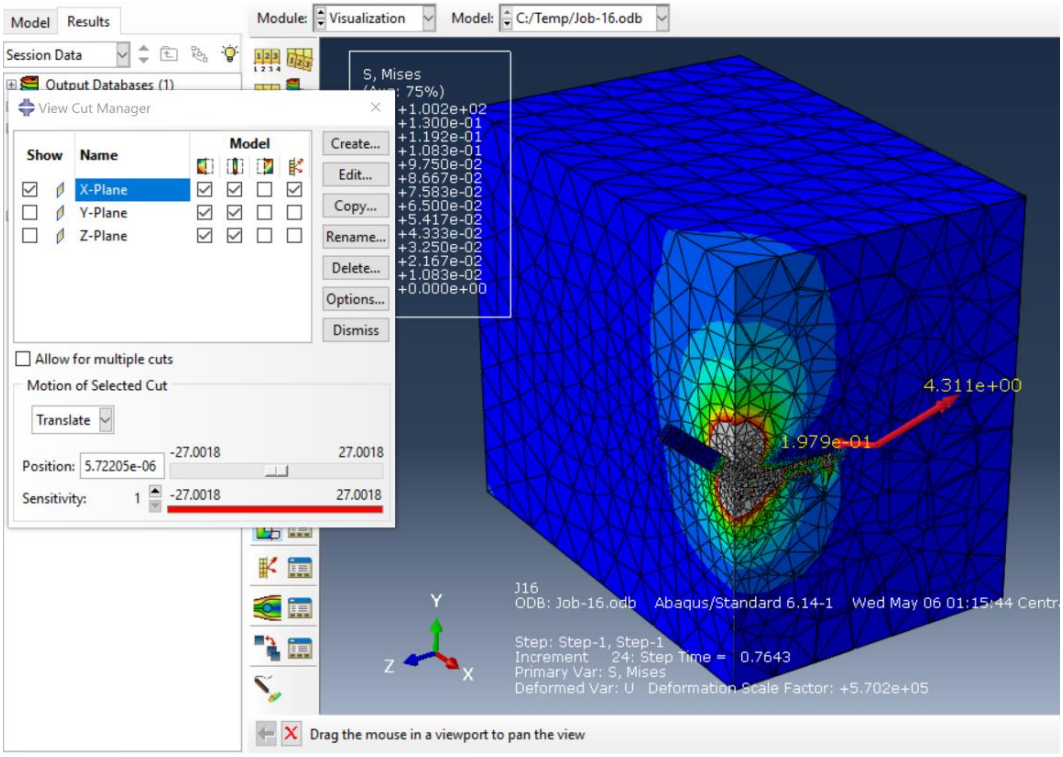

Figure 48. ABAQUS internal force for 0.5%

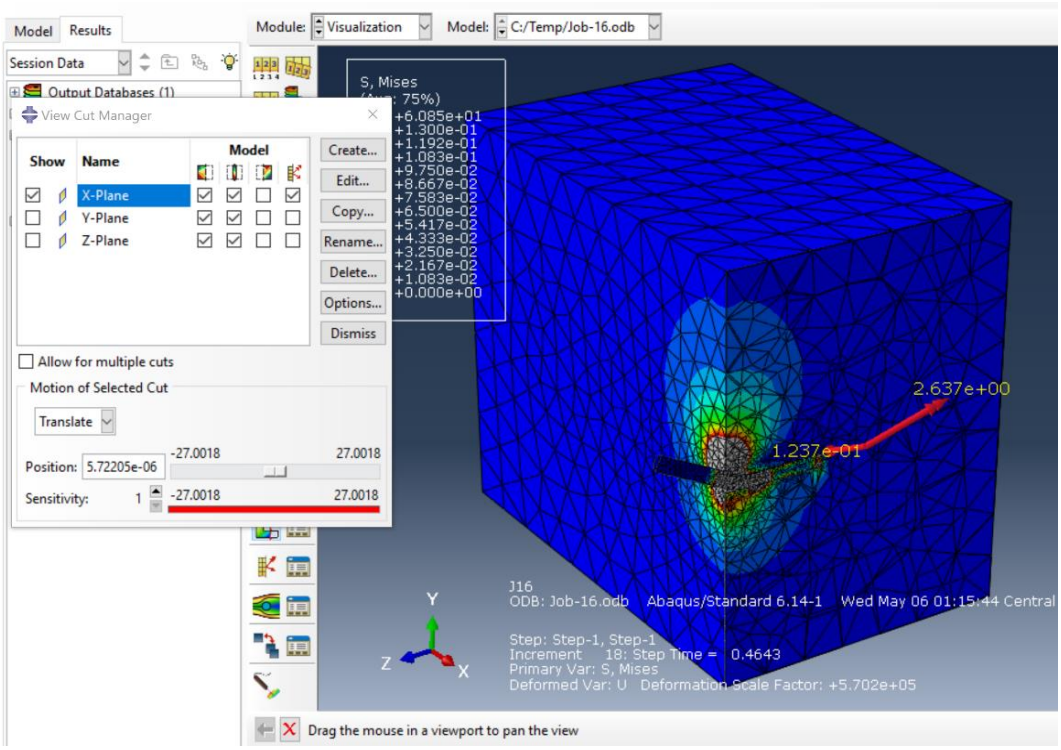

Figure 49. ABAQUS internal force for 1.0%

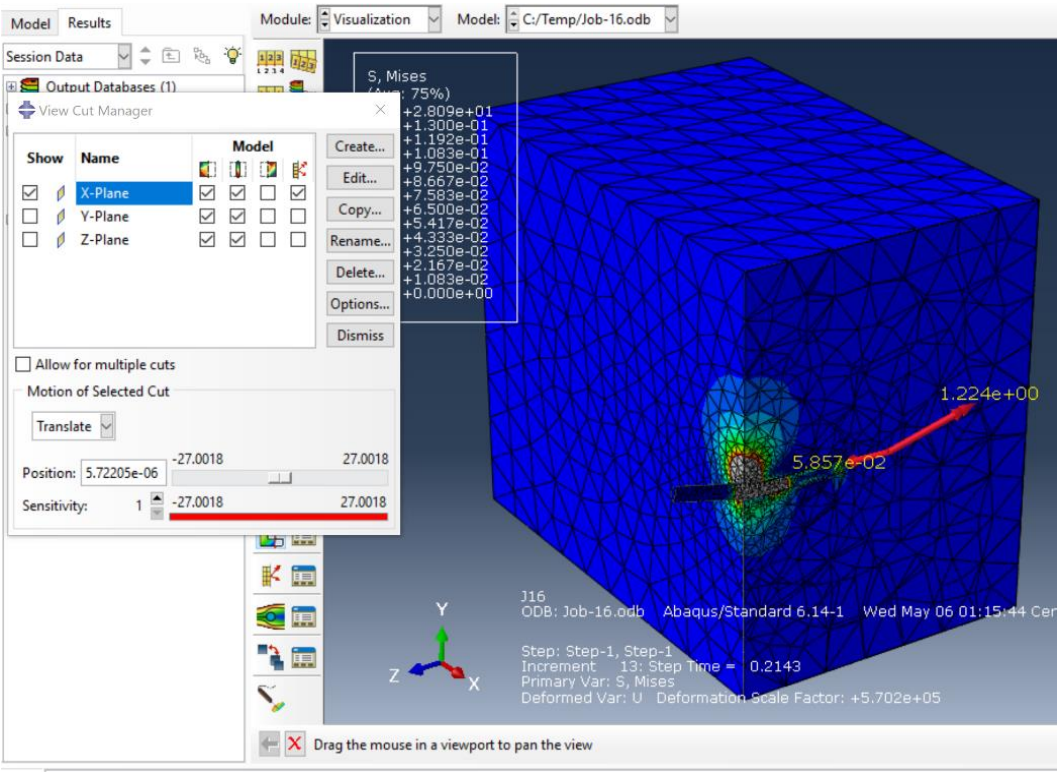

Figure 50. ABAQUS internal force for 1.5%

Figures 51-54 shows that there is a tensile force generated even when the anchors within the SYN-FRC beam is loaded in shear. The prior researches agree with the fact that when anchors are loaded in shear, the significant forces develop in the shear direction along with minor tensile forces and moment due to small eccentricity (Eligehausen et al. 2006). With an increase in fiber reinforcement, there is an increase in the resistance of the tensile force by the polypropylene fibers within concrete.

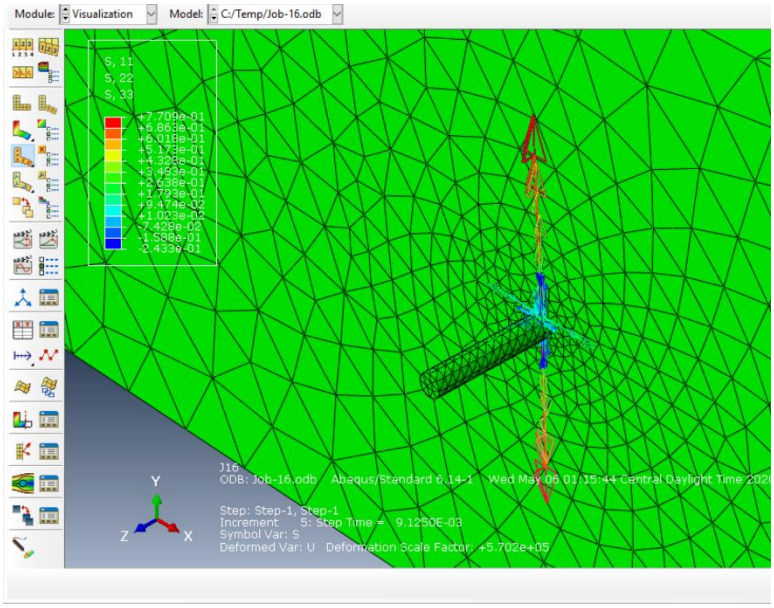

Figure 51. Forces developed in Y-Y direction (SYN-FRC)

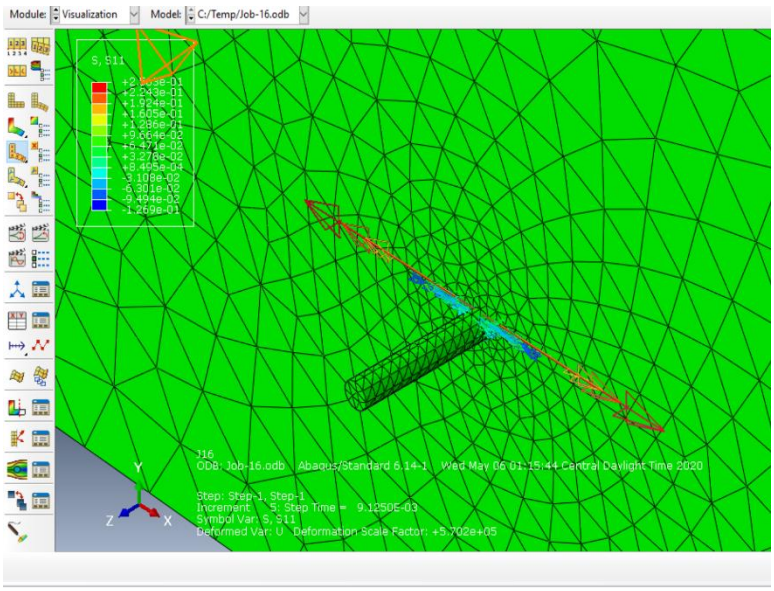

Figure 52. Forces developed in X-X direction (SYN-FRC)

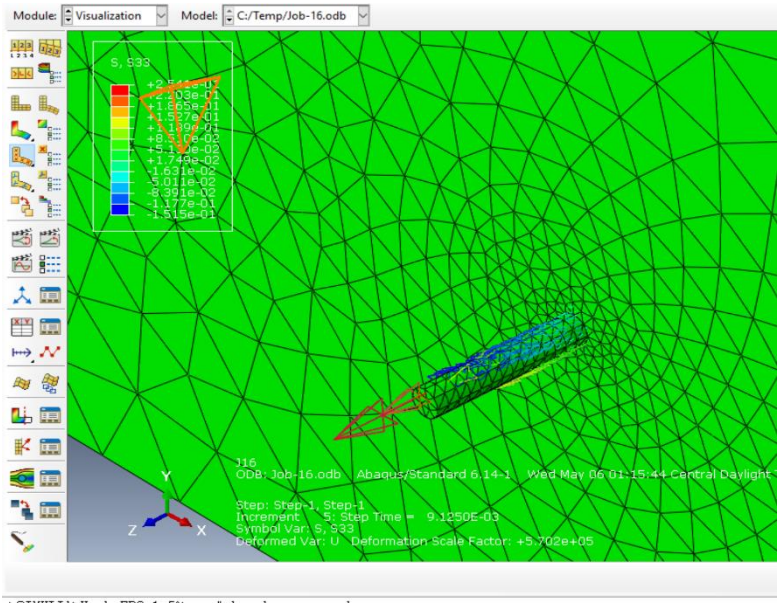

Figure 53. Forces developed in Z-Z direction (SYN-FRC)

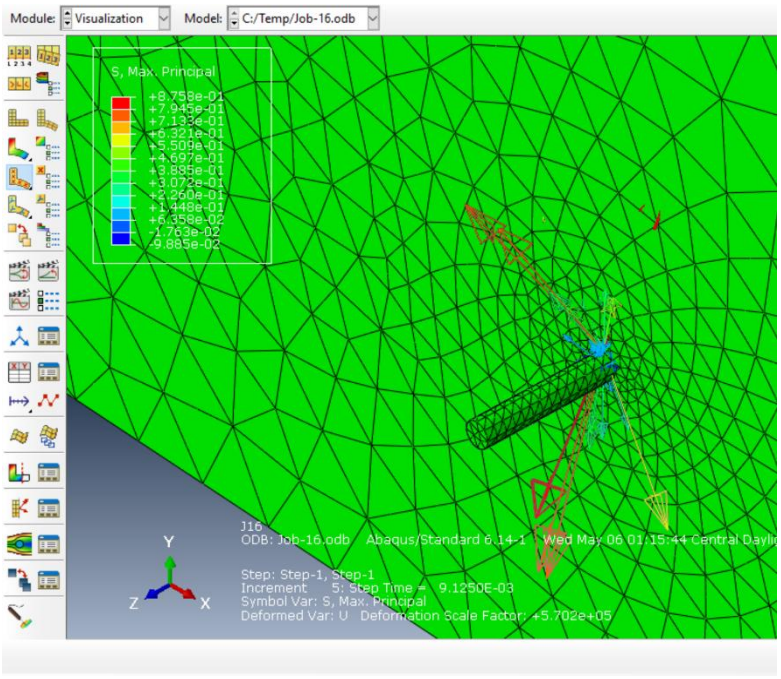

Figure 54. Resultant forces developed in SYN-FRC

Figure 51-54 shows that even though the external force is applied only in positive Y-direction (upward shear), the internal forces are developed in all three directions at the interface of Anchor rod and SYN-FRC.

5.4 Load-Displacement Curve

The displacement for the ABAQUS model is obtained at the very first node above the Anchor rod, as shown in Figure 55. Since the load cell in the experiment is set-up in such an arrangement that the deflection of the SYN-FRC beam near Anchor rod equals with the deflection of Anchor rod.

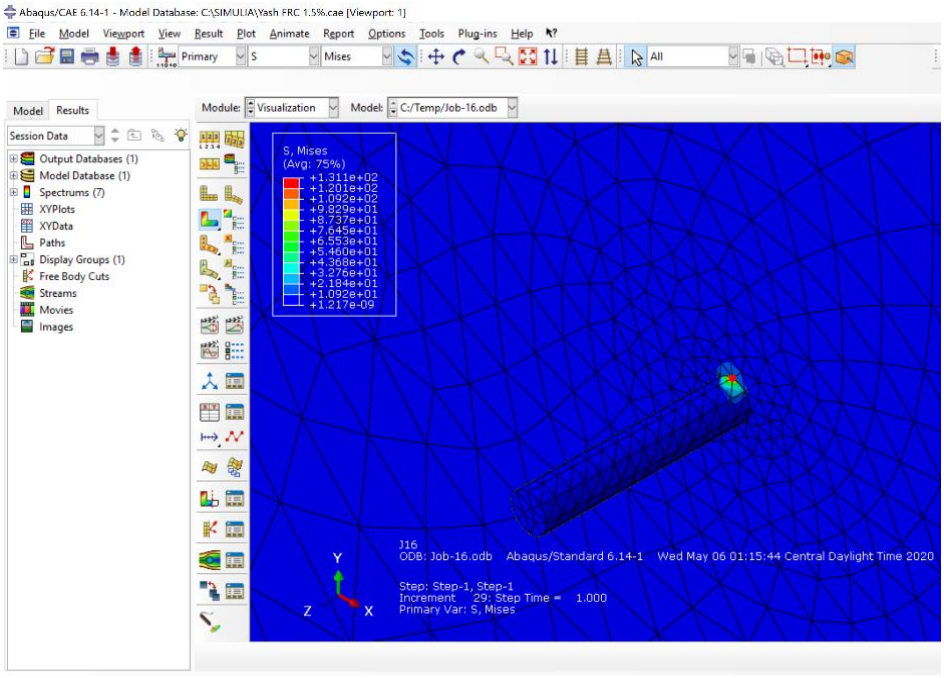

Figure 55. ABAQUS consideration of node for displacement

Table 13. Results for Load - Displacement

Fiber Volume Fraction (%)	Failure Load (lbs.) (Khanfar M. et al. 2019)	Displacement (in.) (Khanfar M. et al. 2019)	Failure Load (lbs.) (Numerical)	Displacement (in.) (Numerical)
0%	23939	1.155	25500	1.15
0.50%	23372	0.995	25000	1.0
1.00%	10694	0.571	12200	0.57
1.50%	6506	0.229	7565	0.23

Figure 56 shows the load-deflection curve from the numerical analysis. The graph is obtained by obtaining deflection against time graph and load against time graph. Merging these two graphs gives us a load-deflection curve.

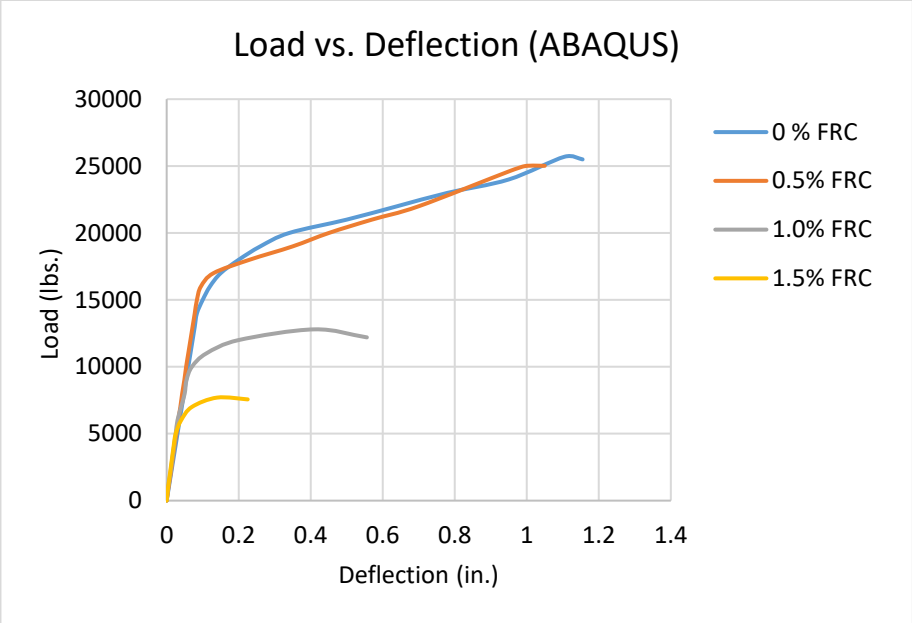

Figure 56. Numerical load-displacement curve

Figure 57 shows a comparison of the Experiment and the Numerical (FEA) load-displacement behavior. Since the experimental results were plotted for deflection against load, the numerical results are posted in the same manner.

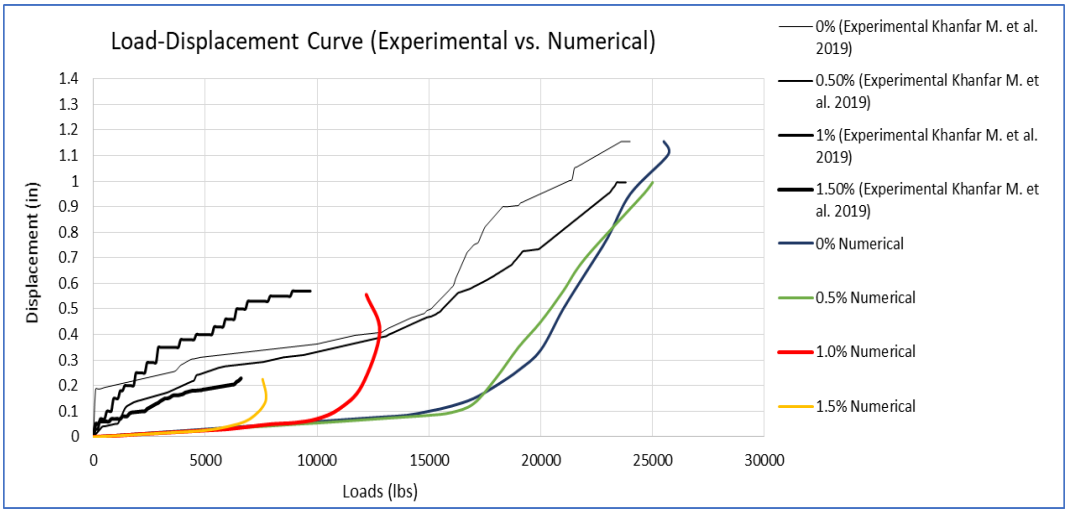

Figure 57. Experiment and Numerical Load-Displacement Curve Comparison

The comparison between experimental and numerical results can only be made when one of the parameters is made constant. Either the load is created equal, and displacement at that load can be compared, or for the same displacement, failure load can

be compared. For this study, the deflection is calibrated to identify the differences in failure loads between experimental and numerical ABAQUS models, as shown in Figure 58.

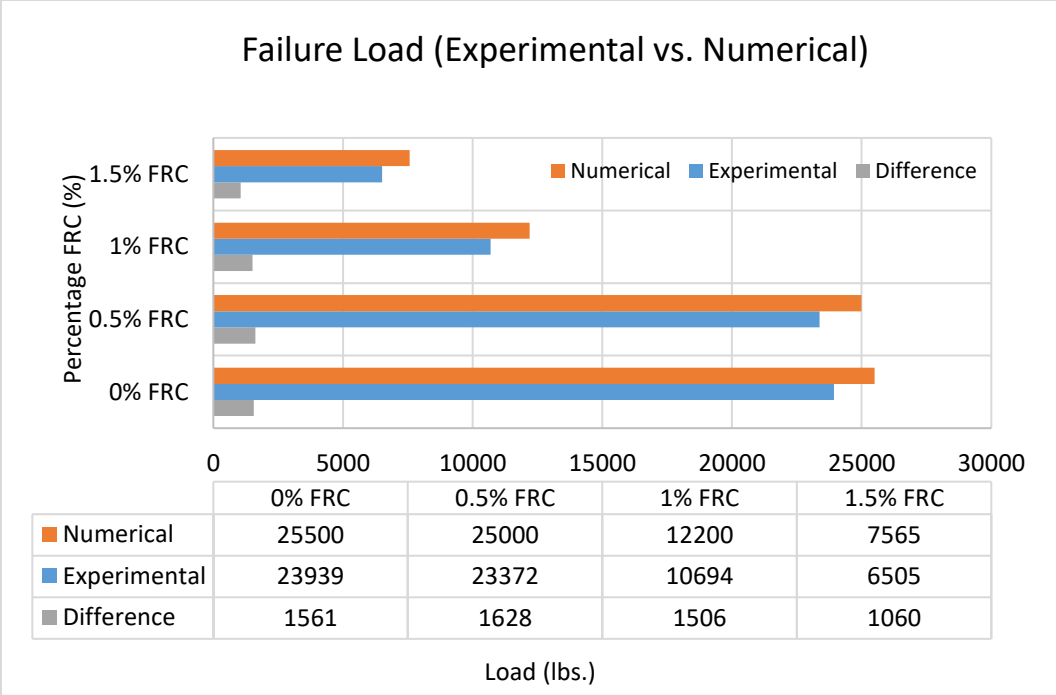

	0% FRC	0.5% FRC	1% FRC	1.5% FRC
Numerical	25500	25000	12200	7565
Experimental	23939	23372	10694	6505
Difference	1561	1628	1506	1060

Figure 58. Experimental and Numerical Failure Load Comparison

Numerical simulations show good agreement with available results from testing of SYN-FRC beam with anchor bolts in shear. The level of failure loads is better simulated than the shape of force-displacement curves. In most cases, simulated displacement at failure load is smaller, or the simulated failure load is higher than that in the corresponding testing. One explanation for this inconsistency might be the way the test setup, such as support and loading equipment, is modeled in the simulation. Initial gaps in the testing equipment are, for example, not considered in the numerical simulations. FEA does not extend the load cycle past the cracking point because of the Concrete Damage Plasticity limits set. This is encouraging because although there is a small difference in values, the model still confirms that Finite Element Analysis is close to the results of a real experiment. Four other Finite Element models are analyzed in the same analysis steps as the Experiment Specimen to give insight into the benefits of different percentages of SYN-FRC beam anchorage. By knowing the realistic displacement that FEA can provide, the software is a reliable tool for structural engineering challenges.

5.5 Parametric Study: Modulus of Elasticity (E)

Modulus of Elasticity (E) of concrete is a crucial factor for estimating the deformation of structural elements, as well as a fundamental factor for determining modular ratio, n, which is used for the design of structural members subjected to flexure. Modulus of Elasticity of concrete is directly proportional to its compressive strength. While empirical equations for predicting Modulus of Elasticity of fiber reinforced concrete have been proposed by many investigators, few equations are considered to cover the entire data. The reason considered is that the mechanical properties of concrete are highly dependent on the properties and proportions of binders and aggregates. In the case of fiber-reinforced concrete, it is more crucial, firstly because the fibers are randomly distributed in the concrete matrix. Secondly, as the fiber reinforcement increases in the concrete, the workability and consolidation of concrete become an issue. Therefore, a wide deviation in results is often encountered. To achieve a standard solution, it is essential to calibrate the behavior of Elastic Modulus exactly as that obtained from the experimental tests.

Table 14 shows the list of studies conducted on various fiber reinforced concrete for the determination of the Modulus of Elasticity. Hence, there is an effort made in this study to find the trend of Modulus of Elasticity for polypropylene fiber reinforced concrete with various percentages of addition by volume to concrete.

Table 14. Database of experimental data (Suksawang N. et al 2018)

	Reference	Type of fiber					L_f, mm	V_f, %			CIS		Strength, MPa		
		Steel	PVA	Polypropylene	Polyolefin	Basalt		≤1	1 to 3.5	3.5 to 10	<1	>1	$f_c' < 50$	$50 \leq f_c' < 100$	$f_c' \geq 100$
1	Pliya et al.[7]			•			6	•				•		•	
		•					30	•				•		•	
2	Lee et al.[20]	•					30, 35, and 50	•	•		•		•	•	
3	Ayub et al.[6]					•	25		•			•		•	
4	Mansur et al.[14]	•			•		30	•	•			•		•	•
5	Altun et al.[17]	•					60	•				•	•		
6	Yang[60]		•				8, 12, 15, and 19	•				•	•		
		•					30, 35, and 60	•				•	•		
7	Yoo et al.[8]	•					30	•	•			•	•	•	
8	Alberti et al.[61]				•		60	•			•		•		
		•					35	•			•		•		
9	Maruthachalam et al.[24]				•		45	•				•		•	
10	Jo et al.[16]	•					60	•	•			•	•	•	
11	Ou et al.[13]	•					5, 6, and 10	•	•		•		•		
12	Abbas et al.[62]	•					8,12, and 16	•	•	•	•				•
13	Alberti et al.[63]				•		48 and 60	•			•		•		
14	Bhargava et al.[5]	•					25 and 50	•	•		•			•	
15	Suhaendi and Horiguchi[64]			•			6 and 30	•				•		•	
		•					30	•				•		•	
16	Naaman et al.[65]	•					30 and 50			•	•		•	•	•
17	Noushini et al.[66]		•				6 and 12	•				•		•	
18	Neves and Fernandes de Almeida[23]	•					30	•	•		•	•	•	•	
19	Hsu and Hsu[23]	•					60	•				•		•	
20	Thomas and Ramaswamy[18]	•					30	•	•			•	•	•	
21	Ayub et al.[9]					•	25	•	•			•	•	•	
22	Alberti et al.[67]				•		60	•	•		•		•		
23	LaHucik et al.[68]	•					60	•			•		•		
				•			40 and 50	•			•		•		
					•		48 and 58	•			•		•		
24	Najm[69]	•					6 to 60	•	•	•	•	•	•	•	•
				•			19		•			•	•		

Figure 59 shows the numerical analysis stress-strain graph from which the Modulus of Elasticity (E) can be computed. The graph for stress against strain was obtained by merging the data from stress against time and strain against time in ABAQUS.

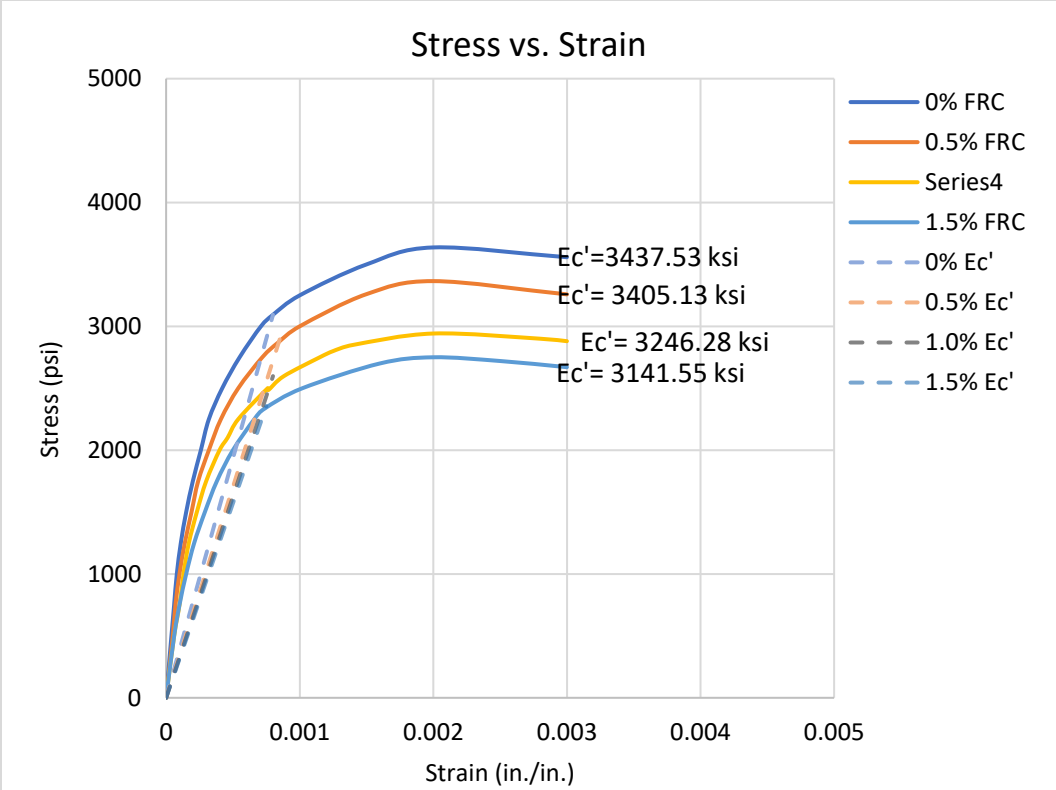

Figure 59. ABAQUS Stress-Strain graph

The graph shows a decrease in the Modulus of Elasticity (E). The strength of concrete is defined by its compressive, tensile, and rupture strength. Since the Modulus of Elasticity for plain concrete is a function of only compressive strength, it is difficult to evaluate the effective Modulus of Elasticity of SYN-FRC. Equation 7 shows the formula to assess the Elastic Modulus for plain concrete (ACI 318-14).

$$E_c = 57000\sqrt{f'_c} \quad \text{.....(7)}$$

Researchers with a previous study on fiber reinforced concrete have developed empirical formulas to evaluate the Modulus of Elasticity. With different types of fiber reinforcement like steel fiber, polypropylene, macro-polyolefin, basalt, and polyvinyl alcohol (PVA) fibers, the empirical formulas can be found in Table 15.

Table 15. List of Empirical Formulas for Modulus of Elasticity (E) and type of fibers

Researcher	Empirical Formula	Type of Fiber
Maruthachalam et al. 2013	$E_c = 361.54V_fS_p + 38{,}534$	Polyolefin fiber
Aslani and Natoori, 2013.	$E_c = 0.242E_{cp} + 1.25V_fS_p$	Steel fiber
Aslani and Samali, 2014.	$E_c = E_{cp} - 31.177V_f$	Polypropylene fiber
Nakin and Salam, 2018.	$E_c = 57{,}000\,\lambda_{vf}\sqrt{f_c'}$ $\lambda_{vf} = 1$ (if C/S > 1) $\lambda_{vf} = (1 + 0.7^{\wedge}lvf)/2$ (if C/S < 1)	Steel, Polypropylene, Macro-polyolefin, Polyvinyl Alcohol (PVA), and Basalt fibers

Where,

C/S = Coarse aggregate weight/Sand aggregate weight

S_p = aspect ratio for fiber (Length of Fiber/Diameter of Fiber)

V_f = Volume fraction of fiber, %

λ_{vf} = Fiber effect factor

Figures 60-62 show the comparison of Modulus of Elasticity (E) with different fiber dosage and strength properties of concrete. It also shows the Modulus of Elasticity obtained through empirical formula (Equation 7) and that obtained from ABAQUS analysis.

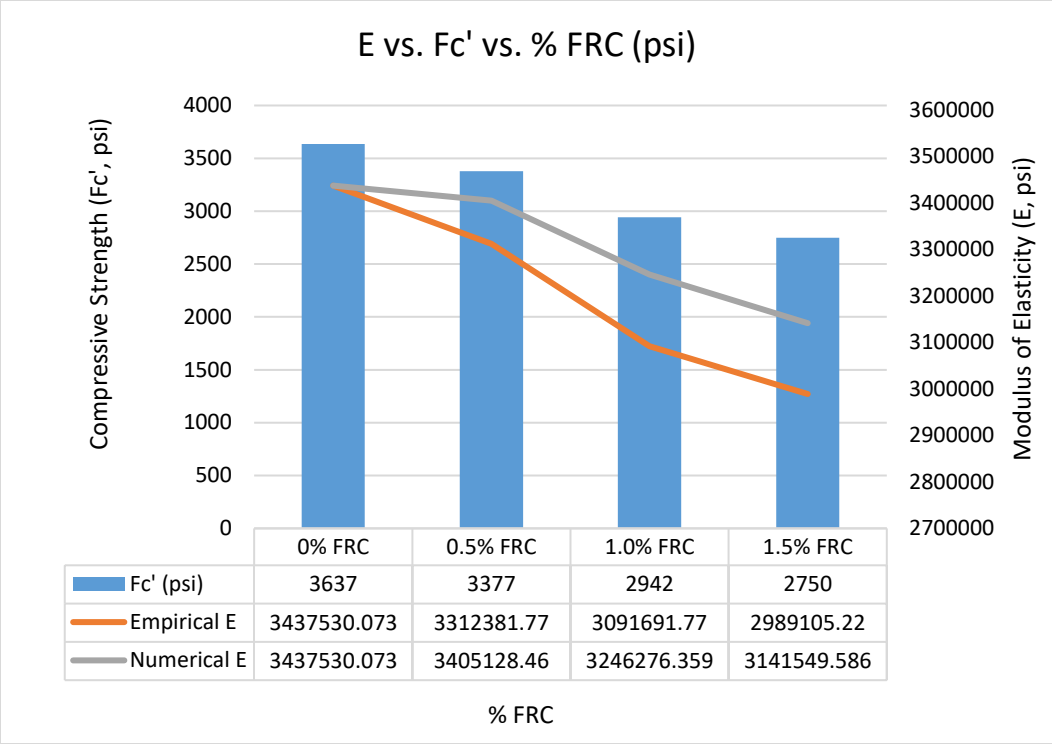

Figure 60. Compressive strength against Modulus of Elasticity

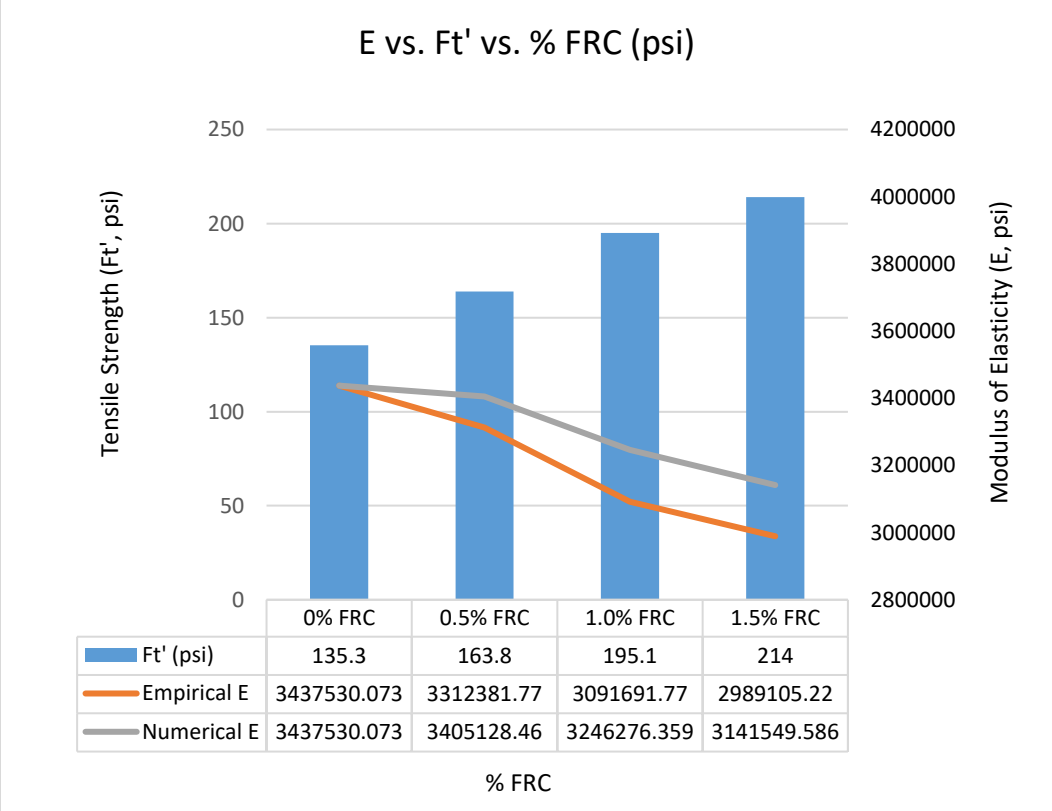

Figure 61. Tensile strength against Modulus of Elasticity

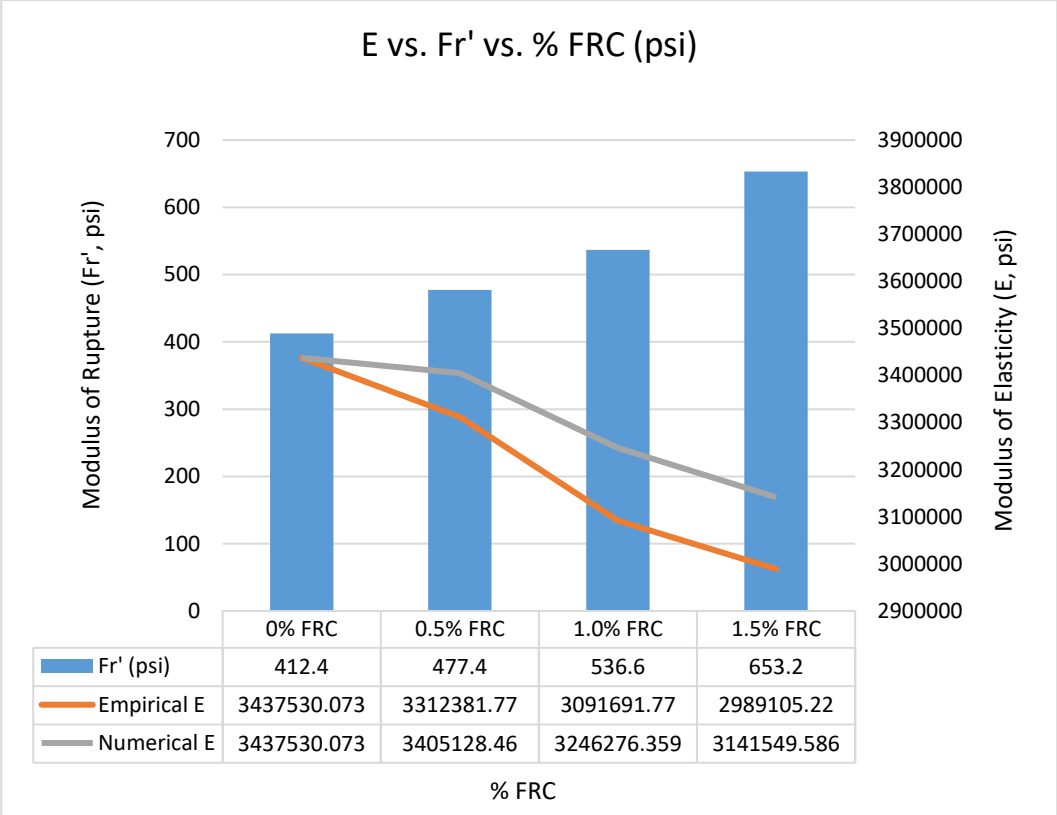

Figure 62. Rupture strength against Modulus of Elasticity

A vast difference is observed between the empirical and numerically obtained Elastic Modulus (E), although both decrease with fiber reinforcement. The trend for the decline for Modulus of Elasticity from an empirical viewpoint can be understood easily as the Elastic Modulus is dependent on compressive strength, and therefore, as the compressive strength decreases, so does the Elastic Modulus (Equation 7). But since a higher Modulus of Elasticity is noticed from the numerical analysis, even though it decreases with increasing fiber dosage, it is essential to compare these because we need to estimate the amount of increase for both empirical computation and dosage of fiber reinforcement. Therefore the efforts are made in this study to modify the equation to compute Elastic Modulus for polypropylene fiber reinforced concrete. Figure 63–65 shows the difference in the stress-strain behavior for the model if it is designed with empirical and that with effective Modulus of Elasticity for 0.5%, 1.0%, and 1.5% fiber reinforcement, since 0% reinforcement means concrete behavior is similar to plain concrete.

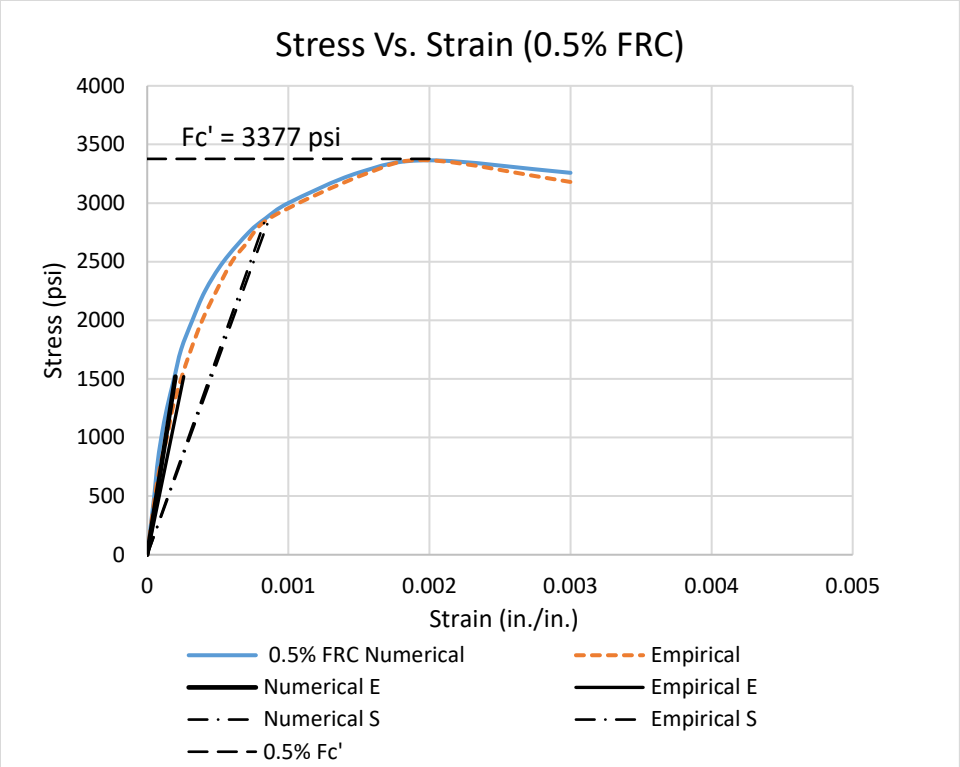

Figure 63. Comparison between Empirical and Numerical Elastic Modulus (0.5% FRC)

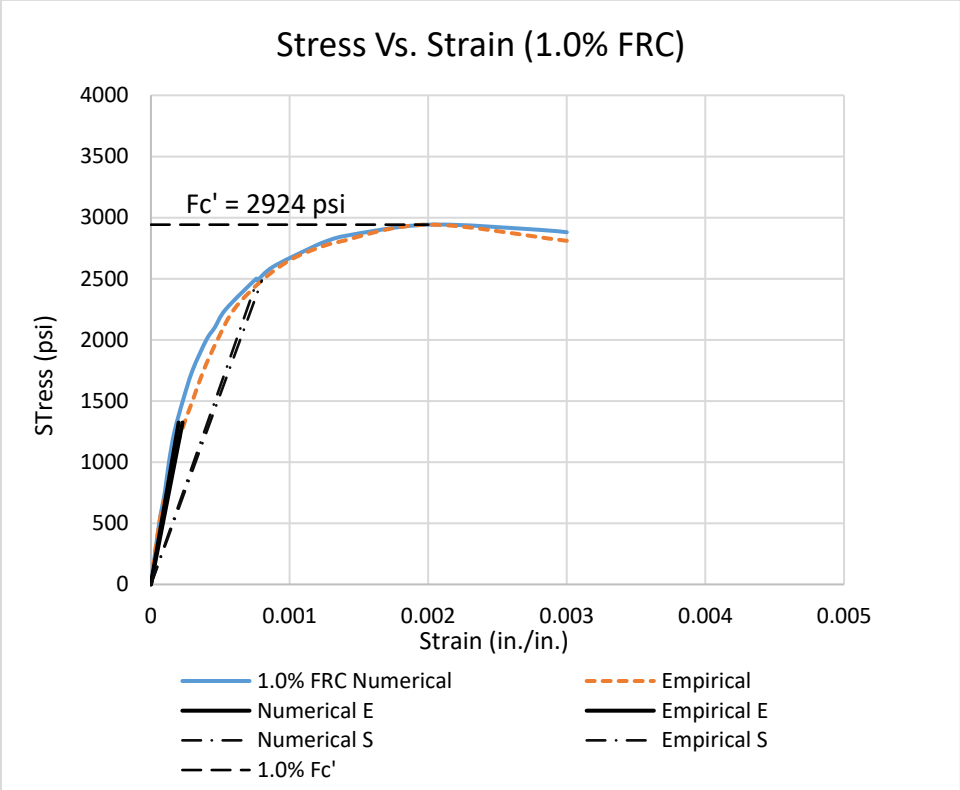

Figure 64. Comparison between Empirical and Numerical Elastic Modulus (1.0% FRC)

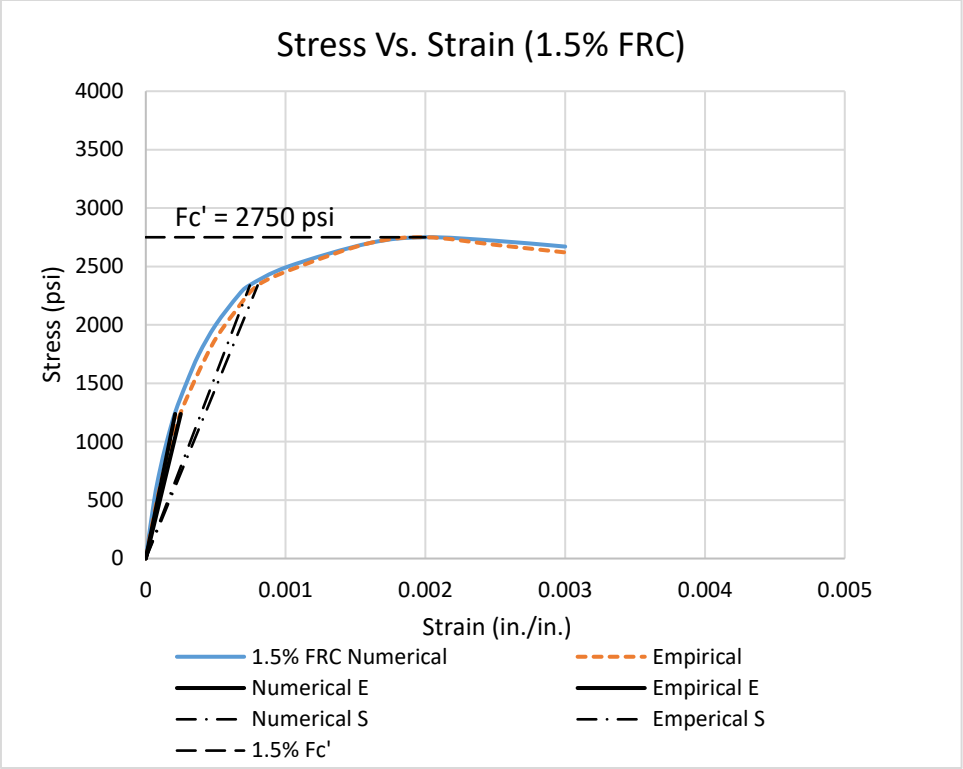

Figure 65. Comparison between Empirical and Numerical Elastic Modulus (1.5% FRC)

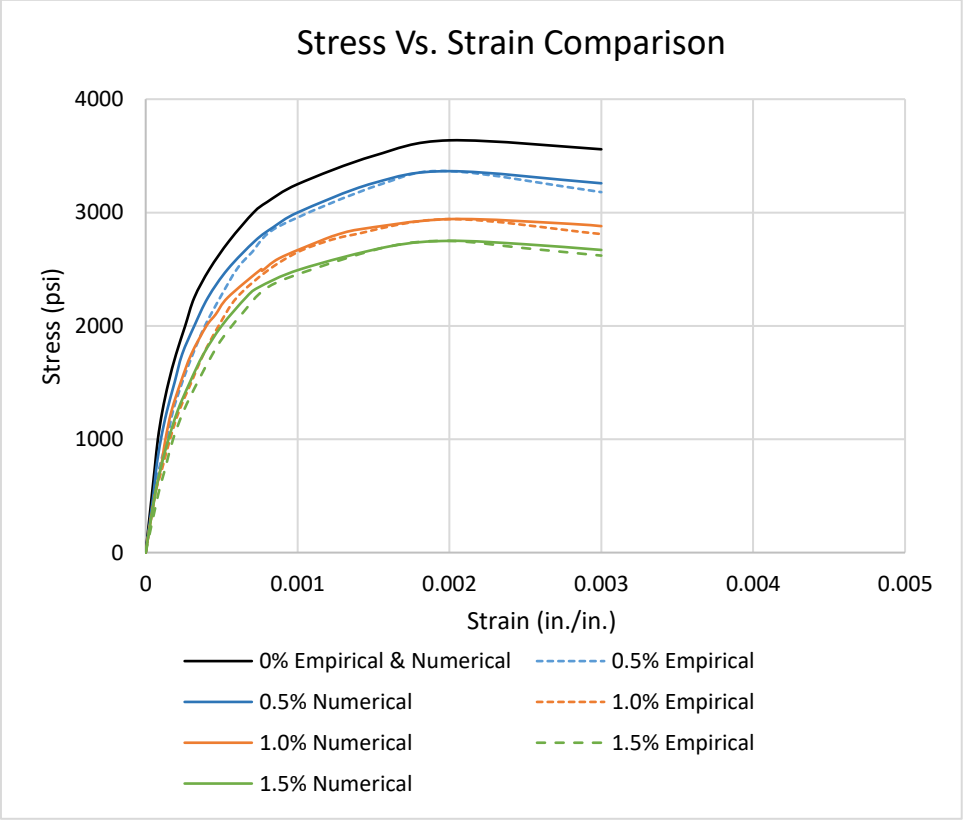

Figure 66. Comparison between Empirical and Numerical Stress-strain relationship

Figure 63-65 shows the stress-strain curve for empirical and numerical analysis for 0.5%, 1.0%, and 1.5% FRC beam. It is also observed that the curve meets at a strain of 0.002, where the compressive strength of concrete is computed from the stress-strain graph. This is observed because the experimental result for the compressive strength of concrete is input directly for the numerical analysis. Hence, there is no change in the compressive capacity of concrete.

Compared to the empirical stress-strain curve, the numerical curve has a slightly more inclined slope for Elastic Modulus (E). Since Modulus of Elasticity is obtained by taking the slope of the line from origin till the point where 45% strength of concrete is attained, it is challenging to compute small strain at corresponding stress. Therefore, to evaluate correct strain and to obtain Elastic Modulus, a check with Secant Modulus (S) is done. The Secant Modulus is obtained to confirm the Elastic Modulus. The Secant Modulus is measured as the slope of the line from the origin to any point in the non-elastic region, mostly where 85% strength of concrete is attained. The Elastic Modulus is then evaluated by considering the Secant Modulus, as shown in Table 16.

Table 16. Computation for Modulus of Elasticity, Empirical, and Numerical

Empirical computation from ABAQUS (E = 57000 x √fc') (psi)								
% Volume Fiber	Compressive Strength Fc' (psi)	Empirical Stress (σ = 0.45 Fc') (psi)	Empirical Strain (Ɛ) (in./in.)	Elastic Modulus (E=σ/Ɛ) (psi)	Empirical Stress (σ' = 0.85 Fc') (psi)	Empirical Strain (Ɛ') (in./in.)	Secant Modulus (S=σ/Ɛ) (psi)	Elastic Modulus (E = S/0.85) (psi)
0%	3637	1636.65	0.000476	3438340.336	3091.45	0.00106	2921900.56	3437530.07
0.50%	3377	1519.65	0.000459	3310784.314	2870.45	0.00102	2815524.50	3312381.77
1.00%	2942	1323.9	0.000428	3091779.542	2500.7	0.00095	2627938.00	3091691.77
1.50%	2750	1237.5	0.000414	2989130.435	2337.5	0.00092	2540739.44	2989105.22
Numerical Computation from ABAQUS (E) (psi)								
% Volume Fiber	Compressive Strength Fc' (psi)	Empirical Stress (σ = 0.45 Fc') (psi)	Empirical Strain (Ɛ) (in./in.)	Elastic Modulus (E=σ/Ɛ) (psi)	Empirical Stress (σ' = 0.85 Fc') (psi)	Empirical Strain (Ɛ') (in./in.)	Secant Modulus (S=σ/Ɛ) (psi)	Elastic Modulus (E = S/0.85) (psi)
0%	3637	1636.65	0.000476	3438340.336	3091.45	0.00106	2921900.562	3437530.07
0.50%	3377	1519.65	0.000446	3404996.639	2870.45	0.00099	2894359.191	3405128.46
1.00%	2942	1323.9	0.000408	3244852.941	2500.7	0.00091	2759334.90	3246276.36
1.50%	2750	1237.5	0.000394	3141660.32	2337.5	0.00088	2670317.148	3141549.59

Table 17 shows the computation of the percentage increase of Modulus of Elasticity against the fiber dosage for 0.5%, 1.0%, and 1.5%.

Table 17. Computation for Modulus of Elasticity (E)

Percentage fiber by volume (Vf) (%)	Compression Strength (fc', psi) (A)	Empirical Modulus of Elasticity Ec = 57000 x√fc'(psi) (B)	Numerical Modulus of Elasticity (psi) (C)	Δ = (C) -(B) (psi) (D)	Percentage of difference(%) $(E) = \frac{(D)}{(B)} \times 100$
0	3637	3437530.07	3437530.07	0	0
0.5	3377	3312381.77	3405128.46	92746.69	2.80
1	2942	3091691.77	3246276.36	154584.59	5.00
1.5	2750	2989105.22	3141549.59	152444.37	5.10

This is to compute the trend line to calibrate empirical Modulus of Elasticity with that of numerical. Figure 67 shows the percent increase in Elastic Modulus for the increasing dosage of fiber reinforcement.

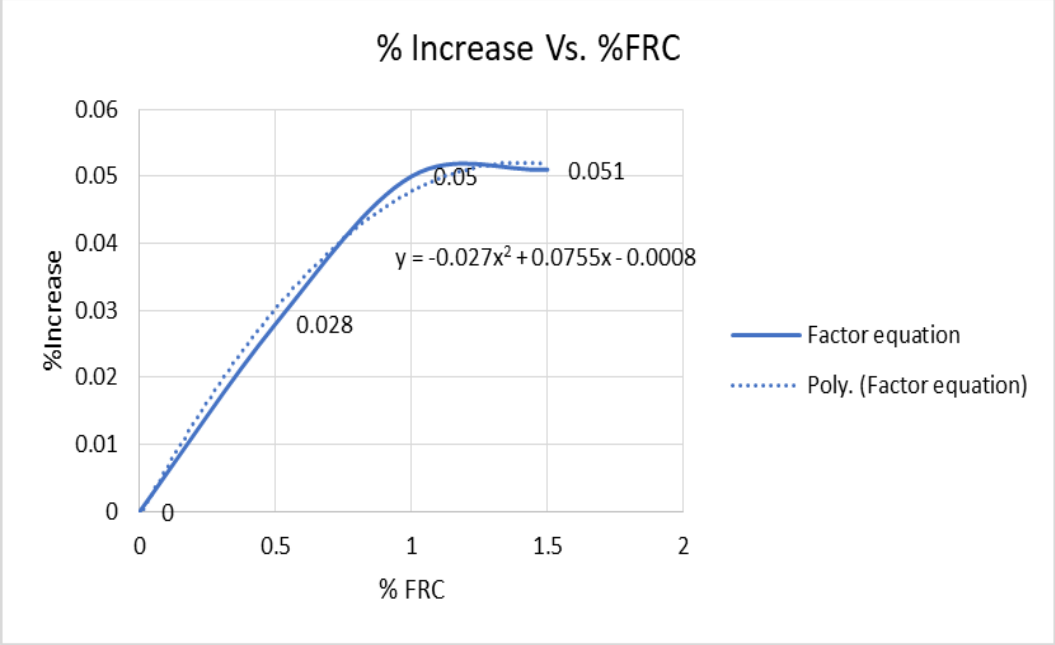

Figure 67. The trend line for computation of factor of increase

The proposed equation for the Modulus of Elasticity (E) for polypropylene fiber reinforced concrete for the numerical simulation is given by,

$$E = 57000 \times \lambda \times \sqrt{fc'} \text{ (psi)} \quad \ldots\ldots(8)$$

Where, λ = factor for increase of Modulus of Elasticity

$$\lambda = 1 \text{ for } (V_f = 0\%) \quad \ldots\ldots(9)$$

$$\lambda = 1 + 0.0277V_f^2 - 0.0755V_f \text{ for } (0\% < V_f < 2\%) \quad \ldots\ldots(10)$$

V_f = Percentage of fiber by volume (%)

Table 18 is provided to show the evaluated Elastic Modulus with the proposed Equation 7. It also shows the percentage of error with respect to numerically obtained Elastic Modulus.

Table 18. Computation for % error in Modulus of Elasticity (E)

Percentage fiber by volume (Vf) (%)	Compression Strength (fc') (psi) (A)	Empirical Modulus of Elasticity Ec = 57000 x√fc'(psi) (B)	λ = 1 - 0.027Vf2 + 0.0755Vf (C)	Proposed Modulus of Elasticity Ec = 57000x λ x√fc'(psi) (D)	Numerical Modulus of Elasticity (psi) (E)	Difference (D) - (E) (F)	% Difference ((F) / (E)) * 100
0	3637	3437530.07	1	3437530.07	3437530.07	0.00	0.000
0.5	3377	3312381.77	1.031	3415065.605	3405128.46	9937.15	0.292
1	2942	3091691.77	1.0485	3241638.821	3246276.36	-4637.54	-0.143
1.5	2750	2989105.22	1.0525	3146033.244	3141549.59	4483.66	0.143

5.6 Discussion of Results

5.6.1 Experimental Results

To affirm the adherence of the experimental results used for numerical analysis, a compression test was performed for all dosages of fiber reinforcement. Four separate concrete mixtures were used, which differed by varying amounts of MasterFiber MAC Matrix, a macro synthetic fiber. The differing mixtures had 0%, 0.5%, 1.0% and 1.5% of fibers by volume. The experimental results for this study matched with the previous experimental results. Therefore, the values for concrete Tensile strength and Modulus of rupture were used directly for the numerical analysis. Also, from the previous experimental investigation, the load-deflection graph was taken for its comparison with the numerical study.

5.6.2 ABAQUS Model

Simulations show that fiber reinforcement has a beneficial effect on concrete breakout strength with an anchor in shear. Firstly, it increases the global stiffness of the concrete structure, which means that the risk for splitting of the concrete at the location of the anchor is reduced. Secondly, it increases the confinement in the vicinity of the anchor, which increases the shear capacity of concrete and thereby increase the capacity substantially. With the addition of fibers, the tensile stress applied to the concrete specimens was resisted by the fiber as well. Thus, with an increase in the amount of fibers, both the tensile and Modulus of rupture increased. It's believed that the increasing fibers led to a reduction in workability, which then leads to a reduction in compressive strength. The failure load for the 0% SYN-FRC beam was noticed to be 6.5% more for the numerical analysis compared to the experimental results. However, for the 0.5%, 1.0% and 1.5% of the dosage, a marginal difference of 7%, 14% and 16.3% was noticed respectively. This can be explained by the poor workability and non-uniform distribution of fibers for a higher dosage of 1% and 1.5%. In summary, failure loads at desired deflection from simulations fairly agree with failure loads from testing for SYN-FRC beam anchorage in shear.

5.6.3 Parametric Study Results

Many studies show that with the increasing polypropylene fiber dosage in concrete, the compressive strength of concrete decreases. Since the Modulus of Elasticity is a function of compressive strength of concrete, researches show a slight reduction in Modulus of Elasticity. However, in this study, the ABAQUS model was designed with iterative Modulus of Elasticity to match the behavior to nearest possible with that of experimental results. While the fibers did not directly increase the compressive strength of the concrete, the fibers may have had an indirect effect due to the reduced workability. Reducing the amount of fibers or the maximum size of the aggregate may be implemented to avoid issues with consolidation in future experiments. Although, there is an overall decrease in Modulus of Elasticity noticed with an increasing percentage of fiber reinforcement. The Modulus of Elasticity was increased by 2.8%, 5.0%, and 5.1% for 0.5%, 1.0%, and 1.5% fiber dosage, respectively (compare to the Empirical Equation 7, which is the only function of fc'). This increase might seem insignificant, but the increase can be associated with the confinement of fibers around the Anchor rod. When the Anchor rod is loaded in shear, it is observed that it crushes the concrete depending on the cone of influence and embedment length of the anchor. Concrete being brittle material, gets crushed depending on its compressive strength. While the crack propagates, the fibers resist the tensile force because of its high tensile capacity and hold the concrete just like any steel reinforcement. The deflection is further taken by the fibers till they break, and that's when the breaking point of fiber reinforced concrete is reached. Thus, it is observed that with increasing the fiber reinforcement, more fibers are randomly distributed, and there is a high probability that the tension force is resisted by more fibers than earlier. Therefore, more stress is held up with a lesser strain. Hence, a slight increase in Modulus of Elasticity is noticed, although there is an overall effective decrease.

Chapter 6

CONCLUSION

This research project has resulted in the following conclusions:

1. Concrete shear failure of headed single anchors in SYN-FRC can be simulated with confidence using finite element analyses.

2. The simulations show good agreement with results from physical experiments. The failure load is better predicted than force-displacement curves.

3. The use of mean concrete cylinder compressive strength together with corresponding tensile strength in the concrete damaged plasticity model seems to be most appropriate for simulation of the physical response of concrete structures.

4. The results of this investigation indicated that FEA enables one to predict SYN-FRC structure behavior even after peak load by using a concrete brittle cracking material model. The tension softening of concrete material could reasonably represent the presence of fibers in numerical modeling.

5. The numerical investigations show a minor increase in Modulus of Elasticity even though the compressive strength decreases. For calibration of the Elastic Modulus for numerical analysis with experimental behavior, Equation 8, 9, and 10 are proposed.

RECOMMENDATIONS FOR FUTURE RESEARCH

- Investigation of the behavior of cast-in-place anchors and concrete breakout strength in shear, with varying diameter and anchor embedment length within fiber reinforced concrete.
- Investigate the effect of combined loading in tension and shear for the SYN-FRC strength with high amounts of fiber reinforcement.
- Investigate the effects of Impact loads on post-installed or embedded anchors within fiber reinforced concrete.
- Experimental and Numerical analysis of post-installed or embedded group anchors within fiber reinforced concrete.
- Study the behavior of anchors for vibration analysis for anchors embedded within fiber reinforced concrete.
- Numerical analysis of the effects of using various types of post-installed anchors within fiber reinforced concrete.

(1) Vsa = n*Ase,v * futa

(2) Vsa = n*0.6 * Ase,v * futa

Vsa = The nominal strength of an anchor bolt for shear (psi)
Ase,v = The effective cross-sectional area of an anchor in shear, (in^2)
futa = Shall not be taken greater than the smaller of 1.9*fya* and 125,000 psi
n = Number of studs or anchors in a group.

(3) Vs = n * As * fut

Vs = The nominal shear strength of a single-headed stud or group of headed studs governed by steel strength (lb)
n = Number of studs or anchors in a group
As = The effective cross-sectional area of a stud anchor, (in^2)
fut = Design minimum tensile strength of headed stud steel in tension (psi)

(4) Vcb = Avc*/*Avco * ψed,v * ψc,v * ψh,v *Vb

(5) Vcbg = Avc*/*Avco * ψec,v * ψed,v * ψc,v * ψh,v *Vb

Vcb = The nominal concrete breakout strength in shear of a single anchor (psi)
Vcbg = The nominal concrete breakout strength in shear of a group of anchors (psi)
Vb = basic concrete breakout strength in shear of a single anchor in cracked concrete
Avc = Projected concrete failure area of a single anchor or group of anchors
Avco = Projected concrete failure area of a single anchor
ψc,v = factor used to modify the shear strength of anchors based on the presence or absence of cracks in concrete and presence or absence of supplementary reinforcement
ψec,v = factor used to modify the shear strength of anchors based on the eccentricity of applied loads
ψed,v = factor used to modify the shear strength of anchors based on proximity to edges of the concrete member
ψh,v = factor used to modify the shear strength of anchors located in concrete members with ha < $1.5c_{a1}$

(6) $$G = \sqrt{(\epsilon \cdot \sigma_{t0} \cdot tan\psi)^2 + \bar{q}^2} - \bar{p} \cdot tan\psi$$

G = Flow potential

Є = Flow potential eccentricity

$\bar{q}$ = Effective Mises stress

$\bar{p}$ = The effective stress caused by hydrostatic pressure.

ψ = The dilation angle is measured in the p-q plane at high confining pressure and indicates the ratio between the volume change and the shear strain

σ_{t0} = The uniaxial failure tensile stress

(7) Ec = 57000 √fc'

Ec = Modulus of Elasticity of concrete

fc' = Compressive Strength of Concrete

(8) E = 57000 x λ x √fc'

Ec = Modulus of Elasticity of concrete

fc' = Compressive Strength of Concrete

λ = factor for reduction of Modulus of Elasticity

(9) λ = 1 for (V_f = 0%)

(10) $\lambda = 1 + 0.0277V_f^2 - 0.755V_f$ for ($0\% < V_f < 2\%$)

V_f = Percentage of fiber by volume (%)

REFERENCES

Abaqus 6.11 Theory Manual (2011).

Abolmaali A., Mostafazadeh M. and Ghahremannejad M. 2019, Shear Strength of Synthetic Fiber-Reinforced Concrete Box Culverts, http://www.researchgate.net/ publication/331876695.

ACI Committee 318. Building Code Requirements for Structural Concrete: (ACI 318-14); and Commentary (ACI 318R-14). Farmington Hills, MI: American Concrete Institute, 2014.

Al-Taan, S.A., and A.A. Mohammed, 2010b. Tensile strength of short-headed anchors embedded in steel fibrous concrete. Al-Radidain Eng. J., 18: 35-49.

Aslani, F., and Samali, B., "High Strength Polypropylene Fiber Reinforcement Concrete at High Temperature," Fire Technology, V. 50, No. 5, 2014, pp. 1229-1247. DOI: 10.1007/s10694-013-0332-y

Aslani, F., and Natoori, M., "Stress-Strain Relationships for Steel Fiber Reinforced Self-Compacting Concrete," Structural Engineering and Mechanics, V. 46, No. 2, 2013, pp. 295-322. Doi: 10.12989/sem.2013.46.2.295

ASTM C39 Test Method for Compressive Strength of Cylindrical Concrete Specimens.

ASTM C78 Test Method for Flexural Strength of Concrete.

ASTM C496 Test Method for Splitting Tensile Strength of Cylindrical Concrete Specimens.

Dharan D. and Lal A. 2016. "Study the effect of polypropylene fiber in concrete", International Research Journal of Engineering and Technology (IRJET), Volume: 3, Issue: 6

Dassault Systémes, 2010. Abaqus Analysis User's Manual Volume I-V, Version 6.10, Abaqus INC.

Eligehausen, R., "Anchorage to Concrete by Metalix Expansion Anchors," University of Stuttgart, Germany, Behavior, and design of fastenings with bonded anchors: numerical analysis and experimental verification

Eligehausen R, Bouska P, Cervenka V, Pukl R, 1992. Size effect of the concrete cone failure load of anchor bolts. In: Bazant, Z.P. (Editor), Fracture Mechanics of Concrete Structures, pp. 517-525, Elsevier Applied Science, London, New York.

Fuchs, W., R. Eligehausen, and J.E. Breen, 1995. Concrete capacity design (CCD) approach for fastening to concrete. ACI Structural. J., 92: 73-94.

Khanfar M. 2019, Experimental investigation of concrete breakout strength of anchors in shear within fiber reinforced concrete, the University of Texas at Arlington.

Mohod M. et al. 2015, “Performance of Polypropylene Fiber Reinforced Concrete”, https://www.researchgate.net/publication/304247224

Mostafazadeh, M., and A. Abolmaali. 2016. “Shear behavior of synthetic fiber reinforced concrete.” Adv. Civ. Eng. Mater. 5 (1): 371–386. https://doi.org/10.1520/ACEM20160005.

Ozbolt J., Gambarelli S. and Hoffman J. 2017, “Bonded Anchors under sustained load: 3D Finite Element Study”, https://www.researchgate.net/publication/320491081

Ramli, R., and E.T. Dawood, 2011b. Study of hybridization of different fibers on the mechanical properties of concrete. Asian J. Applied Sci., 4: 489-492.

Ramujee K. et al. 2013, “Strength Properties of Polypropylene Fiber Reinforced Concrete”, DOI: 10.7324/ijerat.2018.3199

R. Azzawi, N. Varughese, Flexural behavior of preflex sfrc-encased steel joist composite beams, *Results in Engineering*, Results in Engineering 7 (2020) 100122.

Segle P., Strömbro J., Wulff A., Kölfors J., Larsson A., and Persson R. 2013 Numerical simulations of headed anchors break in reinforced and non-reinforced concrete structures, www.stralsakerhetsmyndigheten.se

Suksawang N., Wtaife S., Alsabbagh A. 2018, “Evaluation of Elastic Modulus of Fiber-reinforced Concrete”, https://www.researchgate.net/publication/322904509.

Vidyaranya K. 2019, Experimental Investigation of Concrete Breakout Strength of Anchors in Tension within Fiber Reinforced Concrete, the University of Texas at Arlington.